Biomaterials Advances 154 (2023) 213652

Contents lists available at ScienceDirect

Biomaterials Advances

journal homepage: www.journals.elsevier.com/materials-science-and-engineering-c

Towards modular engineering of cell signalling: Topographically-textured microparticles induce osteogenesis via activation of canonical hedgehog signalling

Fatmah I. Ghuloum [a,b], Lee A. Stevens [c], Colin A. Johnson [d], Natalia A. Riobo-Del Galdo [a,d,e], Mahetab H. Amer [a,*]

[a] School of Molecular and Cellular Biology, Faculty of Biological Sciences, University of Leeds, Leeds, United Kingdom
[b] Department of Biological Sciences, Faculty of Science, Kuwait University, Kuwait City, Kuwait
[c] Low Carbon Energy and Resources Technologies Research Group, Faculty of Engineering, University of Nottingham, UK
[d] Leeds Institute of Medical Research, Faculty of Medicine and Health, University of Leeds, Leeds, UK
[e] Astbury Centre for Structural Molecular Biology, University of Leeds, UK

ARTICLE INFO

Keywords:
Extracellular matrix
Hedgehog signalling
Mesenchymal cells
Microparticles
Microtopography
Osteogenesis
Topography

ABSTRACT

Polymer microparticles possess great potential as functional building blocks for advanced bottom-up engineering of complex tissues. Tailoring the three-dimensional architectural features of culture substrates has been shown to induce osteogenesis in mesenchymal stem cells *in vitro*, but the molecular mechanisms underpinning this remain unclear. This study proposes a mechanism linking the activation of Hedgehog signalling to the osteoinductive effect of surface-engineered, topographically-textured polymeric microparticles. In this study, mesenchymal progenitor C3H10T1/2 cells were cultured on smooth and dimpled poly(D,L-lactide) microparticles to assess differences in viability, cellular morphology, proliferation, and expression of a range of Hedgehog signalling components and osteogenesis-related genes. Dimpled microparticles induced osteogenesis and activated the Hedgehog signalling pathway relative to smooth microparticles and 2D-cultured controls without the addition of exogenous biochemical factors. We observed upregulation of the osteogenesis markers *Runt-related transcription factor2* (*Runx2*) and *bone gamma-carboxyglutamate protein 2* (*Bglap2*), as well as the Hedgehog signalling components, *glioma associated oncogene homolog 1* (*Gli1*), *Patched1* (*Ptch1*), and *Smoothened* (*Smo*). Treatment with the Smo antagonist KAAD-cyclopamine confirmed the involvement of Smo in *Gli1* target gene activation, with a significant reduction in the expression of *Gli1*, *Runx2* and *Bglap2* ($p \leq 0.001$) following KAAD-cyclopamine treatment. Overall, our study demonstrates the role of the topographical microenvironment in the modulation of Hedgehog signalling, highlighting the potential for tailoring substrate topographical design to offer cell-instructive 3D microenvironments. Topographically-textured microparticles allow the modulation of Hedgehog signalling *in vitro* without adding exogenous biochemical agonists, thereby eliminating potential confounding artefacts in high-throughput drug screening applications.

1. Introduction

Significant advancements have occurred in the field of bioengineering in recent years, particularly with regards to cell culture strategies aimed at recreating the native cellular microenvironment and enhancing the relevance of *in vitro* experimental systems. This encompasses factors such as cell-extracellular matrix (ECM) interactions, biochemical signalling gradients, and mechano-transduction. A range of three-dimensional (3D) *in vitro* experimental systems have emerged in the last decade, ranging from organoids and hydrogel matrices, to engineering more complex 3D scaffold-based structures and microfluidics-based devices [1–3].

In the context of bone tissue engineering, tailoring these advanced cell culture experimental systems holds great promise. Native bone surfaces exhibit complex heterogeneous three-dimensional (3D) anisotropic topographies with irregular microstructures [4]. Mesenchymal stem cells (MSCs) can sense these topographical features and secrete distinct ECM components [5,6], which triggers mechanical responses at

* Corresponding author.
E-mail address: m.amer@leeds.ac.uk (M.H. Amer).

https://doi.org/10.1016/j.bioadv.2023.213652
Received 19 July 2023; Received in revised form 19 September 2023; Accepted 3 October 2023
Available online 10 October 2023

the cellular and sub-cellular levels in terms of cell morphology, migration, and tissue organisation [7]. Several studies have employed microscale topographical features to modulate MSCs differentiation *in vitro*, demonstrating that surface topographies can enhance the osteogenic differentiation of MSCs in the presence of classical osteogenic stimuli such as differentiation media or hydroxyapatite [8–10].

Microparticles, also known as microcarriers, provide customisable 3D scaffolds that offer high surface area-to-volume ratio for cell expansion [11]. Whilst microparticles were originally applied for large-scale cell expansion in bioreactors, their applications have since expanded to include tissue engineering and drug delivery applications. We have reported that tailoring micron-sized textured topographies on the surface of polymeric microparticles can effectively induce the osteogenic differentiation of human MSCs (hMSCs) in the absence of exogenous biochemical additives [2]. Nonetheless, the molecular mechanisms underlying this topography-induced osteoinduction are unclear. Understanding the correlation between microparticles-based architectural cues and associated cellular responses on the molecular level is critical to achieve predictable outputs for drug discovery and regenerative medicine applications.

The Hedgehog (Hh) signalling pathway is a key mechanoresponsive signalling pathway that plays an essential role in bone regeneration by promoting osteoblast proliferation, differentiation and maturation [12,13]. Canonical Hh signal transduction in vertebrates involves Hh ligands binding to Patched (Ptch1), leading to Smoothened (Smo) activation and translocation to the primary cilium, where it prevents the processing and stimulates full activation of the Gli family transcription factors. This results in the transcription of Hh-target genes, including *Gli1*, *Ptch1*, and Runt-related transcription factor 2 (*Runx2*) [14]. Several studies have demonstrated that restoring the activity of the Hh signalling pathway in patients with bone fractures promotes bone regeneration [15–17]. In addition, dysregulation of *Gli1* expression, which promotes osteoblast differentiation and suppresses osteoblast maturation, can lead to a decrease in bone mass and delays in bone healing [18].

The mechanical features of culture substrates have been reported to play a key role in modulating cellular responses, including the expression of Hh-related genes [19–21]. Employing biphasic calcium phosphate scaffolds with rough micro- and macro-topographical features significantly increased the expression levels of Gli1 and osteoblast-related genes in human MG63 osteoblast-like cells compared to controls [22]. Lin *et al.* reported that topographical features of titanium surfaces can induce osteogenic differentiation of MG63 cells by upregulating the expressions levels of Hh-related genes, such as *Gli1* and *Smo*, compared to smooth surfaces [19].

Surface engineering of microparticles to create tailored, cell-instructive substrates and direct downstream signalling effectors offers the opportunity to transform cell culture substrates and cell delivery systems from passive components to tailored, functional ones. This offers a powerful tool for developing advanced experimental systems to generate novel biological insights, and a potential alternative to conventional biochemical supplements that can have potential pleiotropic effects on signalling cascades and trigger off-target cellular responses in tissue engineering applications. This study focused on uncovering the role of the Hh–Gli signalling activation in the topographically-induced osteogenesis of mesenchymal progenitors observed on topographically textured microparticles [2]. In this study, our investigation focused on the Hedgehog signalling pathway as the central element of our research hypothesis. Whilst other signalling pathways, such as WNT/NF-κB, also play pivotal roles in osteogenic differentiation [23], we strategically chose to focus on the Hedgehog pathway due to its critical role in early-stage MSCs tissue patterning.

2. Methods

2.1. Fabrication of smooth and dimpled microparticles

Poly(D,L-lactic acid) (PLA) microparticles (Ashland Viatel DL 09 E; Mn 56.5 kDa, Mw 111 kDa, 1, IV 0.8–1.0 dL/g, Ashland Specialties UK) were fabricated using a solvent evaporation oil-in-water emulsion technique as described previously [2]. The organic phase, comprising 1 g of PLA in dichloromethane (20 % (*w/v*) in DCM; Thermo Fisher Scientific) was homogenised (Silverson Machines Ltd., UK) at 3800 rpm for 5 min in an aqueous continuous phase, containing 1 % (*w/v*) of poly (vinyl acetate-*co*-alcohol) (PVA; MW 13–23 kDa, 98 % hydrolysed; Sigma-Aldrich) as stabiliser. The resulting emulsion was stirred at 480 rpm for a minimum of 4 h. The microparticles were then centrifuged at 3500 ×*g* for 5 min and subsequently washed with deionised (DI) water. Microparticles of size range 40–70 μm were collected and subsequently freeze-dried.

To produce dimpled microparticles, 23 % (*w/w*) fusidic acid (FA; 98 %, 5552333, Thermo Scientific Acros) in PLA was incorporated (FA/PLA total content of 10 % *w/v*) at 1200 rpm into PVA solution as previously described [2]. Dimpled microparticles were obtained after FA release in phosphate buffered saline (PBS; 0.1 M, pH 7.4, 0.15 M NaCl, Gibco) for one week at 37 °C.

2.2. Particle size analysis

Samples were dispersed in deionised water, and laser diffraction was used to measure microparticle sizes using a Camsizer XT (Retsch Technology, Germany) for 5 min. For each batch of microparticles, polydispersity index (PDI) was used as a measure of broadness of size distribution. PDI of the fabricated microparticles was defined as the square of the standard deviation divided by their mean diameter. Dimples generated were characterised using ImageJ software by measuring the diameter of a minimum of 250 dimpled microparticles over five independent SEM images for two fabricated batches.

2.3. Brunauer-Emmett-Teller (BET) surface area measurements

Surface area of the fabricated microparticles were calculated as detailed previously [2]. Krypton (Kr) sorption isotherms were carried out using a Micromeritics ASAP 2420 (Micromeritics, Norcross, GA, USA) at −196 °C. Approximately 500 mg samples were degassed under high vacuum (<10 mTorr) at 37 °C for 48 h to remove moisture and other adsorbed gases. As Kr solidifies at higher pressures at −196 °C (>1.77 Torr) [24], sorption isotherms were carried out from 0.10 to 0.65 relative pressure. The specific surface area was acquired from 0.05 to 0.30 relative pressure using the BET model. The pore volume/size distribution was extrapolated from the entire adsorption isotherm (1.75–20 nm) using the Derjaguin–Broekhoff–de Boer model [25].

2.4. Cell culture

C3H10T1/2 cells (ATCC-CCL-226) were kindly gifted by Dr. Hazel Fermor (University of Leeds). C3H10T1/2 cells were maintained in Dulbecco's modified Eagle's culture medium (DMEM; 21969-035, Gibco), which was supplemented with 1 % (*w/v*) L-Glutamine (Gibco), 1 % (*w/v*) Penicillin-Streptomycin (Gibco) and either with 10 % (*v/v*) fetal bovine serum (FBS) (Gibco) (described as "regular media") in routine cell passaging and cell viability assay, or 2 % FBS (described as "serum-reduced media") in all other conducted cell experiments, at 37 °C with 5 % carbon dioxide (CO_2) atmosphere in a humidified incubator. StemPro™ Differentiation Kits (Gibco, UK) were used to confirm tri-lineage differentiation potential of the cells.

2.5. Preparation of microparticles for cell culture

Microparticles were placed in cell-repellent CELLSTAR® 96 well plates (Greiner bio-one) and sterilised with UV light at 254 nm for 30 min at 4×10^4 mJ. The quantities of smooth and dimpled microparticles were calculated to obtain a surface area for cell attachment of 0.32 cm^2 per well. Following this, microparticles were conditioned for 1 h. Cells were seeded at 3×10^4 cells/cm^2 and placed on a plate shaker for 15 min for all conducted experiments. For 2D-cultured controls, cells were seeded at the same seeding density in tissue culture-treated 96 well plates (CytoOne, Thermo Fisher Scientific).

2.6. Assessing cell viability and proliferation

To assess cell viability three days post-seeding, the Viability/Cytotoxicity Assay Kit for Animal Live & Dead Cells (Biotium, UK) was used according to the manufacturer's protocol. Briefly, 1 μM calcein-acetoxymethyl (calcein-AM) and 4 μM ethidium homodimer III (EthD-III) were added per well. Cells were then imaged with an EVOS FL Auto 2 imaging system (Thermo Fisher Scientific) using FITC and TexasRed® filters, respectively.

Proliferation was assessed using PrestoBlue™ Cell Viability Reagent (Invitrogen, UK) at 1-, 3- and 10 days after seeding as per the manufacturer's protocol. Briefly, culture medium was replaced by PrestoBlue™: culture medium (1:9) and incubated for 1 h at 37 °C. After incubation, 100 μL of Prestoblue solution from each well was measured at $\lambda_{exc}/\lambda_{em}$ 560/590 nm using a microplate reader (Polarstar Optima, BMG Labtech).

2.7. Scanning electron microscopy (SEM)

Samples were mounted onto double-sided copper tape (Agar Scientific) and placed on an aluminium pin stub (AGG301, Agar Scientific). Samples were sputter-coated with gold (Cressington sputter coater 208HR) for 4 min prior to imaging, SEM images were taken using a Carl Zeiss EVO MA15 scanning electron microscope (Oxford Instruments) at 10–20 kV.

For sample preparation of cell-containing samples for SEM, cells were fixed three days post-seeding using 2.5 % (*v/v*) glutaraldehyde (STBJ9947, Sigma-Aldrich). This was followed by sequential dehydration using ethanol (Fisher Chemical) at increasing concentrations (10, 25, 50, 80 and 100 %). The fixed aggregates were transferred on aluminium pin stubs (AGG301, Agar Scientific) for SEM imaging. For measuring the average size of cellular protrusions observed on microparticles, three independent images were processed using ImageJ software.

2.8. Immunocytochemistry

Cells were fixed using 3.7 % (*v/v*) formaldehyde then permeabilised using 0.1 % Triton X-100 (Alfa Aesar) for 30 min. To block non-specific binding, incubation in 1 % (*w/v*) bovine serum albumin (BSA, Sigma Aldrich) in PBS was used with either 10 % (*v/v*) normal goat serum (G9023, Sigma-Aldrich) or normal donkey serum (D9663, Sigma-Aldrich), according to the species of the secondary antibody, for 1 h. Cells were then incubated with the primary antibody overnight at 4 °C. The secondary antibody was added for 2 h the following day.

For F-actin staining, cells were stained with ActinGreen™ 488 ReadyProbes™ Reagent (AlexaFluor™ 488 phalloidin) (R37110, Invitrogen) and nuclei were counter-stained with NucBlue™ Fixed Cell ReadyProbes™ Reagent (R37606, Invitrogen). Cells were observed using a Zeiss LSM880 confocal laser scanning microscope (Carl Zeiss, Germany).

The following primary antibodies were used: anti-ADP-ribosylation factor-like protein (ARL13B) mouse monoclonal antibody (1:2000; clone N295B/66, NeuroMab, RRID: AB_2877361), human/mouse GLI-1 affinity purified polyclonal (1:100; AF3455, R&D systems, RRID: AB_2247710), RUNX2 (27-K) antibody (1:500; sc-101145, Santa Cruz Biotechnology, RRID: AB_1128251), anti-osteocalcin (OCN) antibody (1:75; AB10911, Millipore, RRID: AB_1587337), and monoclonal anti-Vinculin (1:70; V4505, Sigma-Aldrich, RRID: AB_477617). Secondary antibodies used in this study were donkey anti-goat IgG (H + L) cross-adsorbed secondary antibody, conjugated to Alexa Fluor 594 (1:500; A-11058, Thermo Fisher Scientific, RRID: AB_2534105), goat anti-rabbit IgG (H + L) cross-adsorbed secondary antibody, conjugated to Alexa Fluor 488 (1:500; A-11008, ThermoFisher Scientific, RRID: AB_143165), and goat anti-mouse IgG (H + L) cross-adsorbed secondary antibody, conjugated to Alexa Fluor 647 (1:500; A-21235, Thermo Fisher Scientific, RRID: AB_2535804).

2.9. Gene expression analysis using real-time polymerase chain reaction (RT-qPCR)

Total RNA was isolated using the RNAqueous™-Micro Kit (Thermo Fisher Scientific) following the manufacturer's protocol. The concentration of RNA in each sample was measured using a NanoDrop™ One Microvolume UV–Vis Spectrophotometer (ThermoFisher Scientific). Reverse transcription of RNA was achieved using the iScript™ Select cDNA Synthesis Kit (Bio-Rad, USA) following the manufacturer's protocol. T100 Thermal Cycler (Bio-Rad) was used following the reaction conditions listed in Table S1. Primer sequences are listed in Table S2. The transcript levels of *Gli1*, *Smo*, *Ptch1*, *Runx2*, osteocalcin (encoded by *Bglap2*), and Glyceraldehyde-3-Phosphate Dehydrogenase (*Gapdh*) were determined using SsoFast™ EvaGreen® Supermix (Bio-Rad), quantified using CFX96 C1000 thermocycler (Bio-Rad) and following the reaction conditions listed in Table S3. No template controls (NTC) for each primer set and no reverse-transcriptase controls (NRT) for each sample were run. Purmorphamine (Miltenyi Biotec) was used as a positive control for *Gli1*, *Smo*, and *Runx2* expression, dissolved in dimethyl sulfoxide (DMSO; 2 μM) in serum-reduced media. Corresponding vehicle controls were prepared as 0.06 % DMSO. Relative expression levels for each gene of interest compared to the housekeeping gene *Gapdh* were determined by using the $2^{-\Delta\Delta Ct}$ method [26] and normalised to the corresponding negative controls along with the standard deviation.

For measuring the expression of *Bglap2*, 2D-cultured C3H10T1/2 cells were treated with osteoinductive media containing dexamethasone (StemPro, Gibco, UK) as positive controls, or untreated as negative controls.

2.10. Western blotting

After 3 days in culture, cells were lysed using CelLytic™ M lysis buffer (C2978, Sigma-Aldrich) containing 1 mM phenylmethyl sulfonyl fluoride (PMSF) (36978, Thermo Fisher Scientific), 1 mM ethylenediaminetetraacetic acid (EDTA; Corning) at pH 8.0, and 1 μL protease inhibitor cocktail (P8340, Sigma-Aldrich). Following incubation on ice for 20 min, the cell lysates were prepared by spinning down at 4 °C, 13,000 rpm for 15 min. Total protein concentrations were determined using the Pierce™ Bicinchoninic acid (BCA) Protein Assay Kit (ThermoFisher Scientific, UK). Cell lysates were analysed by western blot with anti-Gli1 (L42B10) mouse monoclonal antibody (1:800, 2643, Cell Signalling Technology, RRID: AB_2294746) followed by goat anti-mouse IgG (H + L)-horseradish peroxidase (HRP)-linked secondary antibody (1:1000, 1721011, Bio-Rad, RRID: AB_11125936). Detection of the horseradish peroxidase signal was carried out using Clarity Western enhanced chemiluminescence (ECL) Substrate (Bio-Rad), and immunoreactive bands were visualised in a ChemiDoc™ MP Imaging System using Image Lab software (Bio-Rad). Quantification of proteins was carried out by densitometry analysis using ImageJ software (v1.54b) and normalised to loading control HRP-Conjugated GAPDH (1:5000; HRP-60004, Proteintech, RRID: AB_2737588).

2.11. Treatment with KAAD-cyclopamine

Prior to experiments, C3H10T1/2 cells were cultured in serum-reduced media for 24 h, then treated with 300 nM KAAD-cyclopamine (Abcam, UK) or 0.06 % DMSO as vehicle control for 3 days before analysis.

2.12. Fluorescence-based determination of alkaline phosphatase (ALP) activity

Fluorometric quantification of ALP activity at day 3 was carried out using the Alkaline Phosphatase Activity Fluorometric Assay Kit (MAK411, Sigma-Aldrich) following the manufacturer's protocol. Samples were washed with cold PBS and lysed in the ALP assay buffer provided by the kit. Following centrifugation, the supernatant was mixed with 4-methylumbelliferyl phosphate disodium salt (MUP) as a phosphatase substrate and incubated for 30 min at room temperature. Fluorescent intensity was then measured at $\lambda_{exc}/\lambda_{em}$ 360/460 nm using a microplate reader (Polarstar Optima, BMG Labtech). ALP activity for each sample was normalised to its sample background control and expressed as nmol 4-Methylumbelliferyl Phosphate (4-MUP)/mL. ALP activity was normalised by the cell numbers at day 3, expressed as nmol 4-MUP/mL/10^4 cells.

2.13. Statistical analysis

Statistical analysis was performed using GraphPad Prism version 9.3 (GraphPad Software Inc., San Diego, USA). Normality tests were performed, and data was analysed using unpaired Student's *t*-test or the parametric one-way/two-way Analysis of Variance (ANOVA) with Tukey or Dunnett's *post-hoc* tests. All data is shown as mean ± standard deviation (SD), with $p \leq 0.05$ considered the threshold for statistical significance.

3. Results

3.1. Fabrication and characterisation of topographically-textured microparticles

In this study, smooth and topographically-textured microparticles with specific surface micro-scale features were produced by taking advantage of the phase-separation of a sacrificial component using the solvent evaporation oil-in-water emulsion technique, as described previously [2] (Fig. 1A–C).

Emulsion settings, such as homogenization speed and polymer concentration, were optimised (Table 1) so that the fabricated smooth and dimpled microparticles were of a comparable mean diameter, in line with the reported sizes of osteo-inductive microparticles we previously demonstrated to induce osteogenesis in MSCs [2]. The mean diameter of smooth and dimpled microparticles was 53.21 ± 14.18 μm and 50.15 ±

Table 1
Fabrication parameters and properties of microparticles used in this study.

		Smooth	Dimpled
Emulsion settings	FA/PLA ratio	0/100	30/70
	Homogenization RPM	3800	1500
	Polymer concentration (%)	20	10
Particle properties	Particle size (μm)	53.21 ± 14.18	50.15 ± 14.16
	Polydispersity index (PDI)	0.08 ± 0.04	0.07 ± 0.02
	Dimple size (μm)	–	4.60 ± 0.27
	BET surface area (m^2/g)	0.27	0.43
	V_{micro} (cm^3/g)	0.0000096	0.0000175
	V_{meso} (cm^3/g)	0.0001396	0.0002283

Abbreviations: FA, Fusidic acid; PLA, Poly(D,L-lactic acid); BET, Brunauer–Emmett–Teller; RPM, Rotation per minute; PDI, Polydispersity index; V_{micro}, micropore volume; V_{meso}, mesopore volume (we define mesopore volume as the pore volume originating from the pores smaller than 20 nm).

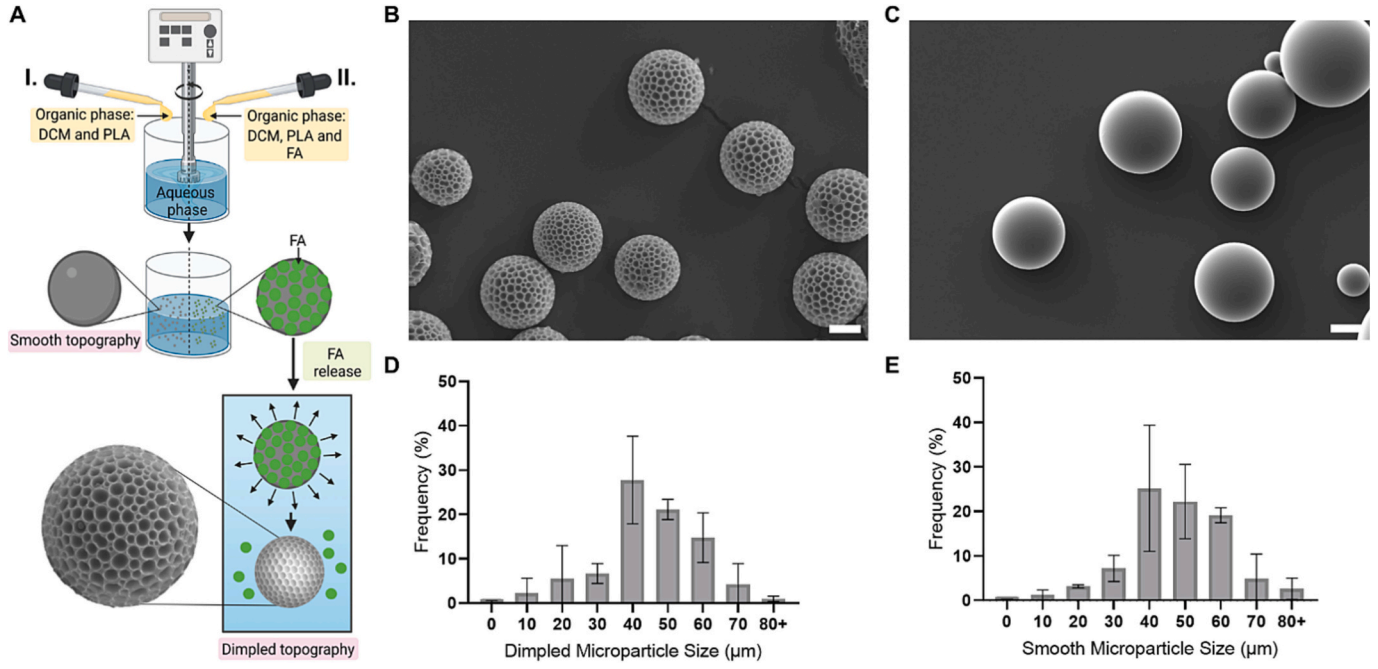

Fig. 1. Fabrication of smooth and topographically-textured (dimpled) PLA microparticles. (A) Schematic representation showing the fabrication of smooth (I) and topographically-textured dimpled microparticles (II) by a modified oil-in-water solvent evaporation emulsion method. The topographical features are engineered using fusidic acid as a phase-separating sacrificial component. (B, C) Representative scanning electron microscopy images of dimpled (B) and smooth (C) microparticles, respectively, fabricated via a solvent evaporation oil-in-water emulsion technique (Scale bar = 20 μm). (D, E) Graphs displaying the microparticle size frequency distribution for the batches used in this study.
Abbreviations: PLA, Poly(D,L-lactic acid); DCM, Dichloromethane; FA, Fusidic acid.

14.16 μm, respectively (Fig. 1D and E) with a mean dimple size of 4.6 ± 0.27 μm on the surfaces of the dimpled microparticles (Table 1).

Surface areas (m^2/g) of microparticles (Table 1) were calculated using the Brunauer-Emmett-Teller (BET) model. To ensure consistency of surface area available for cell attachment across samples, the mass of smooth and dimpled microparticles used was calculated, as previously described [2], to obtain a surface area of 0.32 cm^2 for consistent cell seeding across all 2D and 3D cultures. Both microparticle designs displayed negligible pore sizes, as reflected by their low volumes of micro-pores (Vmicro) and meso-pores (Vmeso) (Table 1).

3.2. Effect of the topographically-textured microparticles on viability, proliferation, and morphology of C3H10T1/2 cells

C3H10T1/2 mouse-derived embryonic fibroblast cells have been widely utilised as a model of multi-potent mesenchymal cells [27,28]. The use of this standard cell line addresses the concern that selective cell attachment from heterogeneous populations of mesenchymal stromal cells may be responsible for the observed osteoinductive response when cultured on the different microparticle designs, rather than being attributable to active cellular differentiation. The ability of these cells to differentiate into osteogenic, adipogenic and chondrogenic lineages was confirmed (Fig. S1).

To elucidate potential signalling mechanisms underpinning the osteo-inductive influence of topographically-textured microparticles [2], serum starvation was employed. Serum starvation is frequently used to synchronise all cells to the same cell cycle phase [29]. Furthermore, serum-starved cells terminate all serum-dependent signalling pathways, which eliminates background when studying the effect of external stimulation on cell behaviour [30,31]. Cells were cultured in low-serum conditions (2 % *v/v* FBS) to allow for cell attachment and avoid stress that may trigger the activation of certain signalling pathways to promote cell survival [32]. To assess cell attachment and viability in the presence of these low serum conditions, cells were cultured in serum-reduced media overnight before seeding on microparticles. The viability of mesenchymal progenitor C3H10T1/2 cells cultured on microparticles in serum-reduced media was compared to cells cultured in regular DMEM culture media supplemented with 10 % FBS using the Viability/Cytotoxicity Assay after 3 days in culture. C3H10T1/2 cells successfully attached to the microparticles and showed high viability under both conditions (Fig. 2A and B). Additionally, visibly smaller cell-microparticle aggregates were observed on dimpled microparticles compared to smooth microparticles in both media conditions.

Cell proliferation was evaluated at days 1, 3, and 10 using the PrestoBlue assay (Fig. 2C). Whilst cell numbers increased on dimpled and smooth microparticles over 10 days of culture, there were no

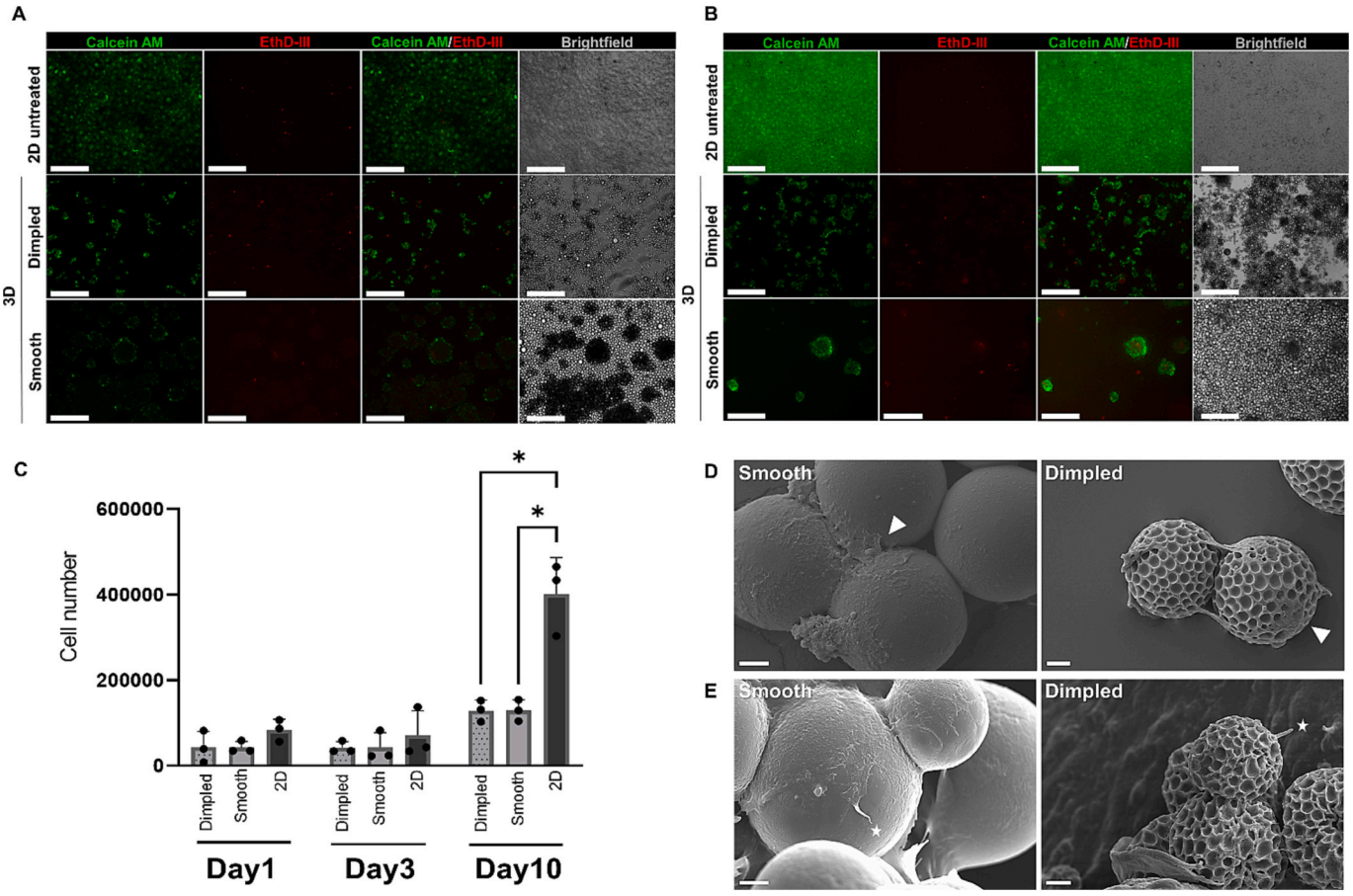

Fig. 2. Viability, proliferation, and morphology of C3H10T1/2 cells on smooth versus dimpled microparticles. (A, B) Representative fluorescence microscopy images showing high viability of C3H10T1/2 cells on smooth and dimpled microparticles 3 days after seeding in (A) serum-reduced (2 % FBS) culture media and (B) in serum-containing (10 % FBS) media. Live cells are stained with calcein-AM (green) and dead cells with ethidium homodimer III (EthD-III) (red). (Scale bar = 300 μm). (C) Proliferation of C3H10T1/2 cells assessed using PrestoBlue on dimpled and smooth microparticle at days 1, 3 and 10 days after seeding. Statistical significance calculated with two-way ANOVA with Tukey's multiple comparisons test. Data represents mean ± standard deviation for three independent repeats. (*$p < 0.05$). (D, E) Scanning electron microscopy images showing the morphologies of C3H10T1/2 cells 3 days after seeding on the smooth and dimpled microparticles. White arrowheads in (D) indicate C3H10T1/2 cells attached to microparticles. White stars in (E) indicate representative cytoplasmic protrusions observed on cells cultured on microparticles (Scale bar = 10 μm).
Abbreviations: Calcein-AM, calcein-acetoxymethyl; EthD-III, ethidium homodimer III.

significant differences observed between cell numbers on the two microparticle designs across all time points. However, cell numbers in 3D-cultured samples were significantly lower than 2D-cultured controls at day 10 ($p \leq 0.05$).

Cells displayed different morphologies when cultured on different topographical designs (Fig. 2D). Cells adopted more elongated morphologies on dimpled microparticles, whilst cells were more spread out on the smooth surfaces. An interesting morphological feature observed was the presence of protrusions projecting from the surface of cells cultured on the microparticles (Figs. 2E and S2). On smooth microparticles, these slender cellular protrusions displayed an average length of 11.21 ± 2.11 μm ($n = 3$), whereas on dimpled microparticles these protrusions were noticeably thicker and shorter, with an average length of 5.59 ± 0.83 μm ($n = 6$).

3.3. Dimpled topographical features alter focal adhesion assembly

The actin cytoskeleton is a dynamic structure that determines cellular shape and regulates its behaviour, with focal adhesions being the primary sites of cell adhesion to a substrate. The formation of stable links with the extracellular matrix leads to integrin clustering and organisation into focal adhesions [33]. To investigate how the arrangement of cytoskeletal proteins was influenced by the changes in 3D topographical features, the organisation of F-actin and vinculin (a membrane cytoskeletal protein found in focal adhesions) in response to different microparticle designs was examined after 3 days of culture and compared to 2D-cultured controls (Fig. 3).

Cell culture on microparticles demonstrated the formation of focal adhesions linked to actin stress fibres (Fig. 3). On the 2D-cultured planar control, cells cultured in serum-reduced medium displayed well-defined focal adhesions, with distinct vinculin-positive streaks organised at the leading edge of the cell but also dispersed widely in the cytoplasm. Network-like actin microfilaments with large stress fibres were observed in 3D-cultured cells (Fig. 3). Perinuclear vinculin-containing focal adhesion sites were visible in cells cultured on smooth microparticles (Fig. 3). In contrast, vinculin was not organised into focal adhesions in cells cultured on dimpled microparticles, but was found distributed throughout the cytoplasm, which may suggest an initial state of F-actin polymerisation [34] or depolymerisation of the actin filaments [35]. This demonstrated that the changes in focal adhesion assembly were correlated with the changes observed in cell morphology.

3.4. Dimpled topographical features induce primary cilia formation

As primary cilium formation has been linked with cellular morphology and organisation of cytoskeletal network [36], 2D and 3D microparticles-based cultures were stained for the ciliary membrane protein ARL13B, a small regulatory Ras GTPase highly enriched in primary cilia [37]. Cilia formation can be affected by sub-micron topographies (i.e. <10 μm) in hMSCs [38], and we therefore investigated cilia formation in C3H10T1/2 cells cultured on microparticles using ARL13B immunostaining.

Cells cultured on dimpled microparticles displayed ARL13B^{+} primary cilia, which were absent in cells cultured on smooth microparticles and few in number in 2D-cultured untreated controls (Fig. 4). To the best of our knowledge, this is the first report of the presence of primary cilia in 3D microparticle-based cultures.

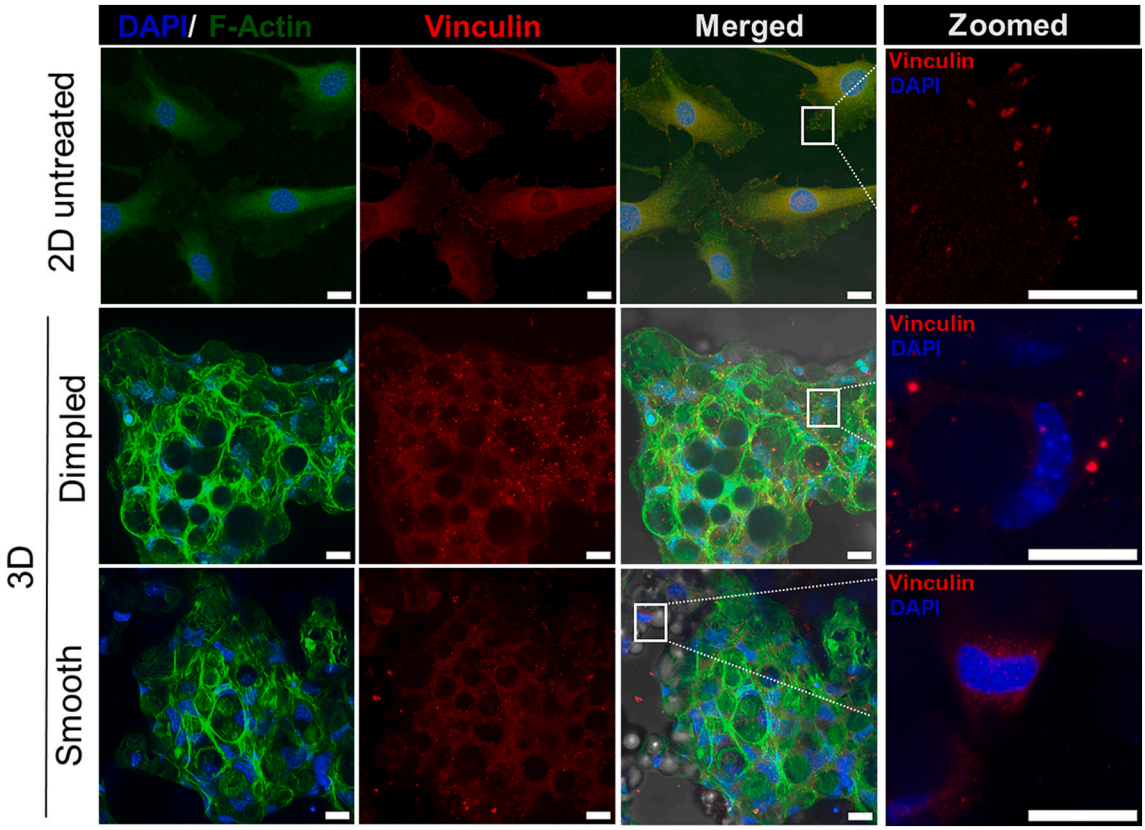

Fig. 3. Three-dimensional topographical features display a differential effect on focal adhesion organisation. Representative immunofluorescence images of C3H10T1/2 cells showing differences in cytoskeletal organisation, stained for vinculin (focal adhesion marker; red), F-actin (green) and nuclei (DAPI; blue). The rightmost panel shows an enlarged view of the vinculin staining observed in the square inset in the merged images. Cells were cultured on two microparticle designs and 2D controls in serum-reduced culture media for 3 days (Scale bar = 20 μm).
Abbreviations: DAPI, 4′,6-diamidino-2-phenylindole.

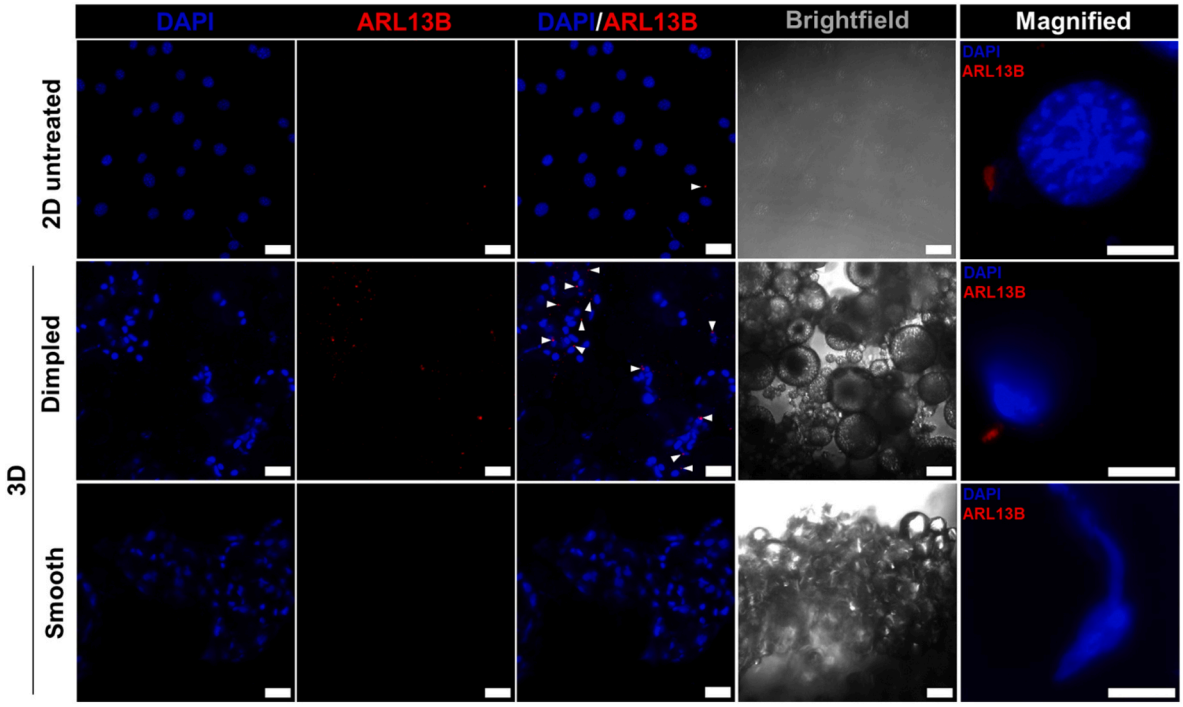

Fig. 4. Representative maximum intensity projection immunofluorescence images of C3H10T1/2 cells stained for ARL13B (ciliary marker; red) and nuclei (DAPI, blue), with positive ciliary staining indicated by white arrows. Cells were cultured on microparticles and 2D untreated cultures in serum-reduced media for 3 days. (Scale bar = 50 μm). Higher magnification images of ciliary staining are also included as "Magnified" (Scale bar = 10 μm).
Abbreviations: DAPI, 4′,6-diamidino-2-phenylindole; ARL13B, ADP-ribosylation factor-like protein.

3.5. Dimpled topographical features induce osteogenic differentiation of C3H10T1/2 cells without the addition of exogenous osteoinductive factors

Given the presence of primary cilia when culturing C3H10T1/2 cells on dimpled microparticles, we next investigated the effects of dimpled topographical features on the primary cilium-associated Hedgehog (Hh) signalling pathway, and how this may influence downstream osteogenic differentiation on these osteo-inductive topographical features [2]. To confirm the osteo-inductive capability of dimpled microparticles using the C3H10T1/2 mesenchymal progenitor cells, we quantified early and late markers of osteogenesis (*Runx2* and *Bglap2* encoding osteocalcin, respectively; Fig. 5A–D). Since Runx2 binds to promoter sequences of bone-specific proteins to regulate osteogenesis [39], Runx2 activation indicates early osteogenic commitment. Positive control cultures were treated with either 2 μM purmorphamine or osteo-inductive media, chemical inducers of *Runx2* [40] and *Bglap2* [41] expression, respectively (Fig. S3). Moreover, ALP activity was significantly elevated in cells cultured on dimpled microparticles when compared with cells cultured on smooth microparticles and untreated controls ($p < 0.0001$, Fig. S4).

Cells cultured on dimpled microparticles displayed a statistically significant increase in *Runx2* expression levels compared to those cultured on smooth microparticles (7.26-fold versus 3.91-fold; $p < 0.0001$) relative to 2D negative controls and normalised to *Gapdh* (Fig. 5A). To further confirm the osteoinductive effect of 3D dimpled topographies on C3H10T1/2 cells without the use of exogenous biochemical supplements, relative expression analysis of *Bglap2* (a mature osteoblast marker) was determined 3 and 7 days after seeding (Fig. 5B and C). Culture on dimpled microparticles significantly upregulated the expression levels of *Bglap2* by 31.87-fold ($p < 0.01$) in C3H10T1/2 cells after 3 days in culture, whereas no significant differences in the levels of *Bglap2* expression by cells cultured on smooth microparticles was observed relative to 2D untreated controls (Fig. 5B). This significant increase in *Bglap2* expression on dimpled microparticles continued to be observed at day 7, with a 23.39-fold increase of *Bglap2* expression levels relative to 2D negative controls. Cells cultured on smooth microparticles for 7 days displayed 8.21-fold increase in *Bglap2* expression relative to 2D untreated controls ($p < 0.0001$) (Fig. 5C).

Immunostaining was also carried out at day 3 to confirm the effect of dimpled topography on RUNX2 expression, and at day 8 to assess OCN expression. Immunostaining also confirmed notably higher expression levels of RUNX2 in C3H10T1/2 cells cultured on dimpled microparticles relative to smooth microparticles. Nuclear localisation of RUNX2 was observed on dimpled microparticles, whereas RUNX2 was retained mostly in the cytoplasm in cells cultured on smooth microparticles (Fig. 5D). Additionally, a markedly higher expression of OCN was observed in the cells cultured on dimpled microparticles relative to smooth microparticles (Fig. 5E). These findings confirmed the enhanced ability of dimpled microparticles to induce osteogenic differentiation of C3H10T1/2 cells without employing exogenous osteo-inductive factors.

3.6. Topographically-induced osteogenesis is associated with the Hedgehog signalling pathway

The Hedgehog signalling pathway is essential in stem cell regulation and development [42]. Given the well-known role of Hh signalling pathway in driving MSCs osteogenic commitment by increasing the expression levels of *Runx2* [43] and boosting osteoblast maturation by upregulation of the expression of osteocalcin [44], we next investigated the involvement of the Hh signalling pathway in the 3D dimpled topography-induced osteogenesis. The expression of Hh signalling pathway-related genes were quantified at day 3 after seeding (Fig. 6).

Interestingly, the trends seen in canonical Hh induced gene expression levels in cells cultured on dimpled microparticles were similar to those observed for osteogenic gene expression at day 3 post-seeding. Expression levels of *Gli1* and *Ptch1*, hallmark target genes of canonical Hh signalling, were significantly upregulated on dimpled microparticles by 17.31-fold ($p < 0.0001$, Fig. 6A) and 2.06-fold ($p < 0.01$, Fig. 6B), respectively, relative to 2D untreated cultures. Remarkably, dimpled microparticles were able to induce *Gli1* expression to a comparable level

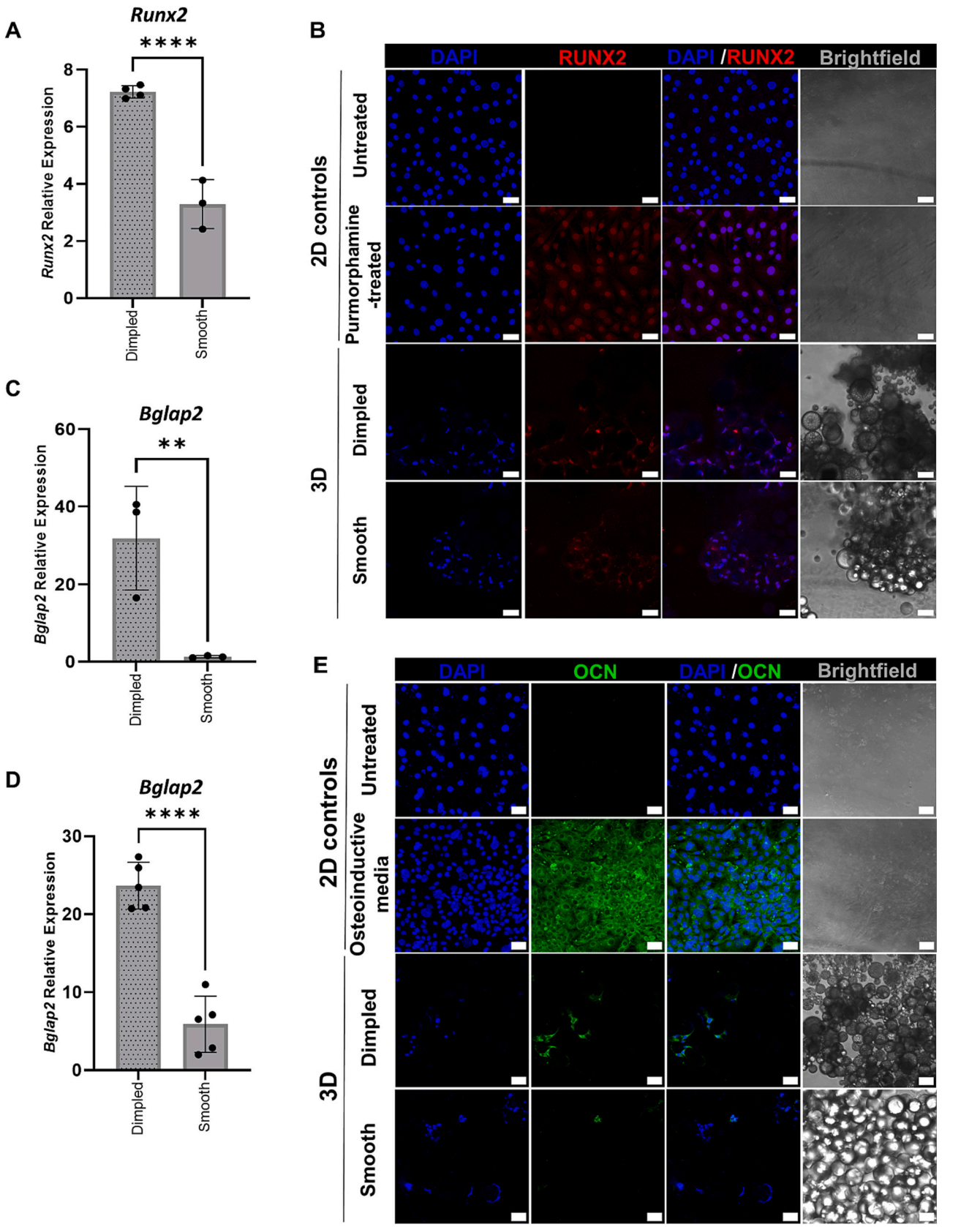

(caption on next page)

Fig. 5. Culture on topographically-textured microparticles induces the expression of early and late markers of osteogenesis without the addition of exogenous osteoinductive factors. (A) Relative quantitative real-time PCR (qPCR) analysis of *Runx2* expression levels after 3 days in serum-reduced media, represented as fold change normalised to *Gapdh* and relative to 2D untreated controls. (B) Representative maximum projection images obtained by confocal microscopy of C3H10T1/2 cells stained for RUNX2 (red) after 3 days (Scale bar = 50 μm) and nuclei (DAPI; blue). 2D-cultured positive controls were treated with 2 μM purmorphamine for 3 days to induce RUNX2 expression. (C–D) Relative qPCR analysis of *Bglap2* expression levels after 3 days (C) and 7 days (D) in in serum-reduced media, represented as fold change normalised to *Gapdh* and relative to 2D untreated controls. 2D positive control were treated with osteoinductive media. (E) Representative maximum projection images obtained by confocal microscopy of C3H10T1/2 cells stained for OCN (green) after 8 days of culture (Scale bar = 50 μm; DAPI; blue), including positive (osteo-inductive) and negative (untreated) controls. Statistical significance calculated with one-way ANOVA with Tukey's multiple comparisons test. Values are means ± standard deviation for 3 independent biological repeats. (*$p < 0.05$, **$p < 0.01$, ****$p < 0.0001$).
Abbreviations: DAPI, 4′,6-diamidino-2-phenylindole; Runx2, Runt-related transcription factor2; Bglap2, bone gamma-carboxyglutamate protein 2; *Gapdh*, Glyceraldehyde-3-Phosphate Dehydrogenase; OCN, osteocalcin.

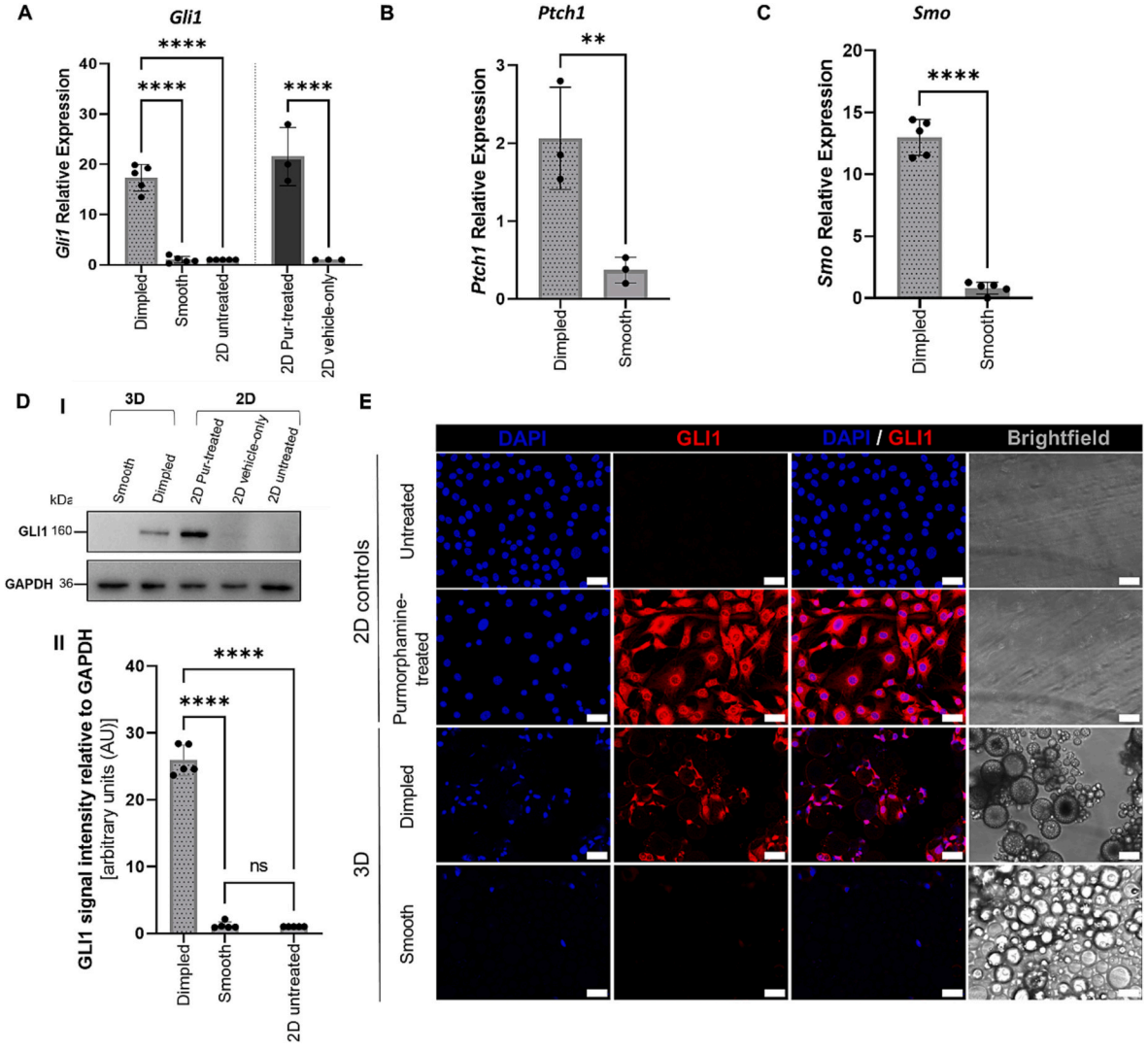

Fig. 6. Dimpled microparticles upregulate the expression levels of Hh-related markers. Relative quantitative real-time PCR (qPCR) analysis of Hh-related genes (A) *Gli1*, (B) *Ptch1* and (C) *Smo* after 3 days in culture in serum-reduced media, represented as fold change normalised to *Gapdh* and relative to 2D controls. Expression levels in 2D purmorphamine-treated controls (2 μM) were calculated relative to 2D-vehicle only controls (treated with 0.06 % DMSO; $n = 3$). (D) Representative Western blot (I) and densitometry analysis performed (II) showing GLI1 expression levels in C3H10T1/2 cells 3 days post-seeding, normalised to GAPDH ($n = 5$). Statistical significance calculated with one-way ANOVA with Tukey's multiple comparisons test for all data, with the exception of 2D controls where unpaired Student's *t*-test was used. Values are shown as means ± standard deviation (*$p < 0.05$, **$p < 0.01$, ***$p < 0.001$, ****$p < 0.0001$). (E) Representative confocal immunofluorescence microscopy images of C3H10T1/2 cells immunostained for GLI1 (red) and nuclei (DAPI; blue). 2D positive controls were treated with 2 μM purmorphamine (Scale bar = 10 μm).
Abbreviations: DAPI, 4′,6-diamidino-2-phenylindole; Gli1, glioma associated oncogene homolog 1; *Ptch1*, Patched1; Pur-treated, purmorphamine-treated; Smo, Smoothened; *Gapdh*, Glyceraldehyde-3-Phosphate Dehydrogenase.

to that observed in 2D positive controls treated with 2 μM purmorphamine, a *Smo* agonist recognised for its ability to induce osteogenesis through the activation of the Hh signalling pathway [40], which showed a 21.54-fold increase in *Gli1* expression relative to the corresponding 2D-vehicle only controls (Fig. 6A). Moreover, the expression level of *Smo*, a central transducer of the Hh signal that is not a target of Gli-dependent transcription [45], was also increased by 12.99-fold in the cells cultured on the dimpled microparticles ($p < 0.0001$, Fig. 6C).

Expression levels of the three Hh signalling-related genes showed no statistically significant differences between smooth microparticles and 2D negative controls. GLI1 protein expression was verified by western blotting and quantified by densitometry analysis at day 3, showing a 25.90-fold increase in GLI1 expression in cells cultured on dimpled microparticles relative to its expression in 2D untreated controls (Fig. 6D).

High GLI1 protein expression was observed on the C3H10T1/2 cells cultured on dimpled microparticles by immunofluorescence staining, similar to that seen in the purmorphamine-treated cells in 2D cultures (Fig. 6E). In contrast, no expression of GLI1 was observed in C3H101/2 cells when cultured on smooth microparticles. This was consistent with the results observed using RT-qPCR and western blotting.

Taken together, this data demonstrates that dimpled topographically-textured microparticles induced the activation of Hh signalling and osteogenesis in the mesenchymal progenitor C3H10T1/2 cells without the addition of exogenous biochemical additives or Hh pathway agonists.

3.7. Osteogenesis induced by dimpled topography is mediated by Smo-dependent Hh signalling pathway

Activation of canonical Hh signalling requires regulated trafficking of proteins into and out of the primary cilium [46]. During pathway activation, Smo accumulates in primary cilia to signal activation of Gli2 and Gli3, which then induce the expression of Gli-target genes, among which Gli1 and Ptch1 are widely recognised [47]. Therefore, we further investigated the role of Smo in the topographically-induced activation of the Hh signalling pathway and osteogenesis. We hypothesised that dimpled topographies sensed by C3H10T1/2 cells lead to Smo-dependent activation of Hh signalling, which upregulates downstream osteogenesis-related genes expression. For this purpose, we quantified the expression levels of *Gli1* and osteogenesis-related genes, *Runx2* and *Bglap2*, with and without the Smo inverse agonist, KAAD-cyclopamine (Fig. 7). The concentration in DMSO was optimised to preserve the textured topographical features of the fabricated microparticles (Fig. S5).

KAAD-cyclopamine treatment resulted in significant decrease in the expression of all three genes under investigation in the cells cultured on dimpled microparticles. Inhibition of Smo using KAAD-cyclopamine significantly prevented *Gli1* upregulation in cells cultured with dimpled topographies at both the transcript and protein levels ($p < 0.0001$, Fig. 7A and B). In the presence of KAAD-cyclopamine, no statistically significant differences in the expression levels of *Gli1* in C3H10T1/2 cells cultured on smooth microparticles were observed.

Pharmacological inhibition of Smo also prevented the previously observed upregulation of osteogenesis-related genes in C3H10T1/2 cells cultured on dimpled microparticles. This was demonstrated by the statistically significant reduction in expression levels of *Runx2* ($p < 0.001$, Fig. 7C) and *Bglap2* in KAAD-cyclopamine treated cells ($p < 0.0001$, Fig. 7D and E). The expression levels of *Bglap2* at day 7 in the presence of KAAD-cyclopamine treatment were significantly reduced to the levels observed in C3H10T1/2 cells cultured on smooth microparticles ($p < 0.0001$, Fig. 7E). Taken together, our results show that the topographical design of microparticles can differentially activate the canonical Hh signalling pathway. Furthermore, our data demonstrates the modulation of osteoinduction, mediated by the canonical Smo-dependent Hh signalling pathway, through engineering cell-instructive 3D microenvironments on topographically-textured microparticles.

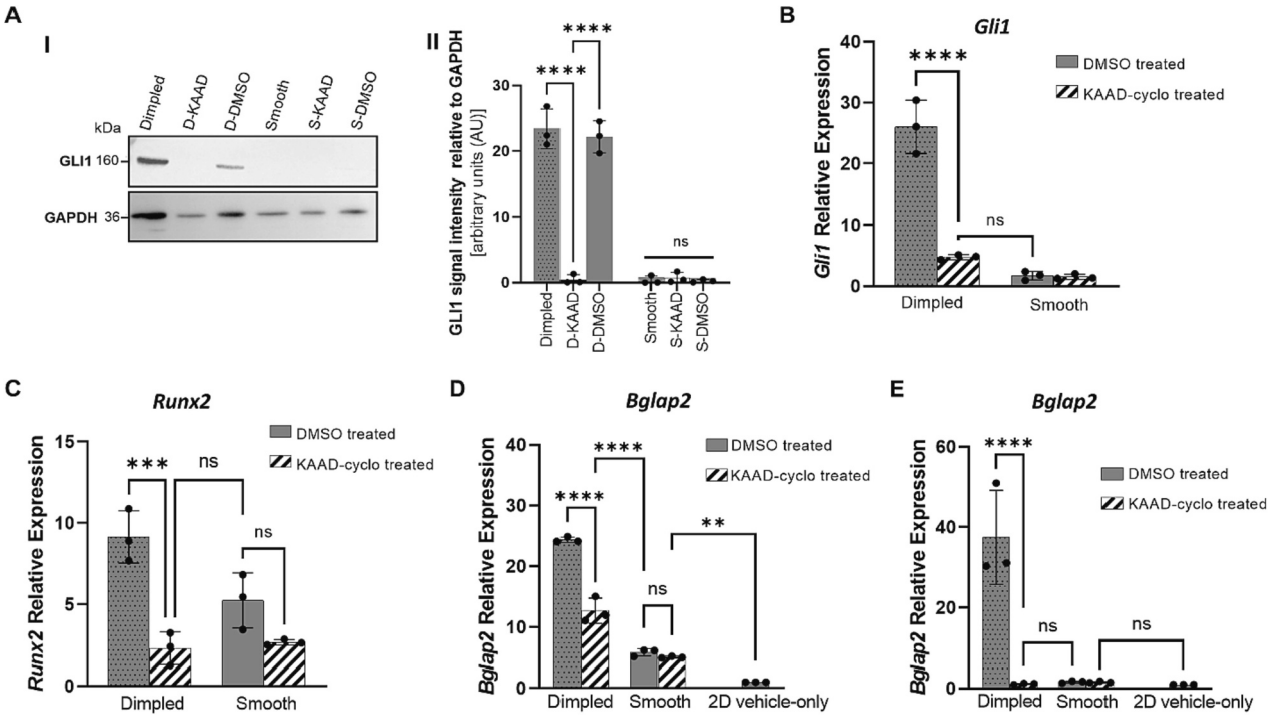

Fig. 7. Hedgehog activation and topographically induced osteogenesis is Smo-dependant. (A) Representative Western blot (I) and densitometry analysis (II) showing GLI1 expression levels in C3H10T1/2 cells after 3 days of 300 μM KAAD-cyclopamine treatment, normalised to GAPDH ($n = 3$). (B–D) Relative qPCR analysis of (B) *Gli1*, (C) *Runx2* and (D, E) *Bglap2* after 3 (D) and 7 (E) days in culture, represented as fold change normalised to *Gapdh* and relative to 2D vehicle-only controls. Statistical significance was determined using one-way ANOVA with Tukey's multiple comparisons test. Values are means ± standard deviation for three independent biological repeats. (**$p < 0.01$, ***$p < 0.001$, ****$p < 0.0001$, ns = no statistically significant difference).

Abbreviations: D-KAAD and S-KAAD, 300 μM KAAD-cyclopamine treated cells cultured on dimpled and smooth microparticles, respectively: D-DMSO and S-DMSO, 0.06 % DMSO-treated cells cultured on dimpled and smooth microparticles, respectively; Gli1, glioma associated oncogene homolog 1; *Runx2*, Runt-related transcription factor2; *Bglap2*, bone gamma-carboxyglutamate protein 2; DMSO, dimethyl sulphoxide; KAAD-cyclo, KAAD-cyclopamine; GAPDH, Glyceraldehyde-3-Phosphate Dehydrogenase.

4. Discussion

Modularity is ubiquitous in biological systems. Polymeric microparticles offer great potential as functional biomaterials-based building blocks for use in bottom-up tissue engineering and advanced culture systems. Topographically-textured microparticles are a powerful tool to direct cell response, and can be customised to add further functionality [48], enhancing their utility. Providing mechanistic insights into how topographical design criteria for microparticles-based environments influence cell signalling opens the door for ex vivo control of cell fate in disease model development. Therefore, the aim of this study was to investigate the Hh signalling-mediated osteogenic differentiation of 3D micro-topographical cues using topographically-textured PLA microparticles in the absence of exogenous agonists. Our study's innovation lies in its focused investigation of the Hedgehog signalling pathway as a mediator of the osteoinductive impact of 3D topographical features in the absence of confounding biochemical factors that are typically added to induce differentiation *in vitro*. This has yielded invaluable insights into the mechanistic underpinnings of how surface-engineered, topographically-textured polymeric microparticles induce osteogenic differentiation. This innovation holds significant promise, as it presents a more physiologically relevant experimental model system that utilises physical cues to modulate Hh signalling without relying on exogenous small molecules. This work demonstrates the potential of utilising patterned microparticles as a physical alternative to biochemical Hh agonists in discovery research.

We demonstrate that the osteo-inductive influence of C3H10T1/2 mesenchymal progenitor cells by dimpled microparticles is mediated by the activation of canonical Hh signalling, as demonstrated by the upregulation of various Hh-related signalling markers and increased primary ciliogenesis, demonstrating the Smo-dependency of osteogenic marker expression (Fig. 8).

When employing microparticles as culture substrates, cell viability and proliferation are critical. The selection of PLA for the fabrication of microparticles in this study served to maintain the integrity of the engineered 3D topographical features, avoiding the degradation and loss of the engineered topographical features in culture [2,48]. C3H10T1/2 cells showed excellent attachment and viability on the microparticles. Additionally, increased proliferation rates in 2D controls compared to their 3D counterparts was observed. This aligns with previous studies reporting that cells display reduced proliferation rates in 3D cultures compared to those cultured in 2D, and are matrix-dependent [2,49–51]. Proliferation rates in 3D-cultured systems better represent *in vivo* models than 2D cultures [52]. The differences in C3H10T1/2 cell morphologies when cultured on smooth and dimpled microparticles agree with those we previously reported using human MSCs [2], which are hypothesised to be due to preferential use of different mechano-transducers to adapt to the different physical microenvironments [53]. Human MSCs attachment on dimpled microparticles was reported to be mediated primarily via integrins α_5 and $\alpha_v\beta_3$, unlike those cultured on smooth microparticles [2]. Integrins are known to connect to the primary cilium via the actin cytoskeleton, and focal adhesions are clusters of integrins and transmembrane receptors that mechanically link the ECM to the actin cytoskeleton [54]. In this study, we utilised a larger number of smooth microparticles compared to dimpled microparticles to maintain consistency of surface area across samples, thereby isolating topography as the primary variable under investigation. This may account for the differences observed in cell-microparticles aggregate size (Fig. 2). This is consistent with previous research, in which it has been reported that varying microparticles seeding density controlled the number of microparticles incorporated within 3D cell-microparticles aggregates [55].

Remarkably, C3H10T1/2 cells also displayed cytoplasmic projections extending from the surface of cells cultured on dimpled microparticles (Fig. 2E). These may be similar to the 'micro-spikes'

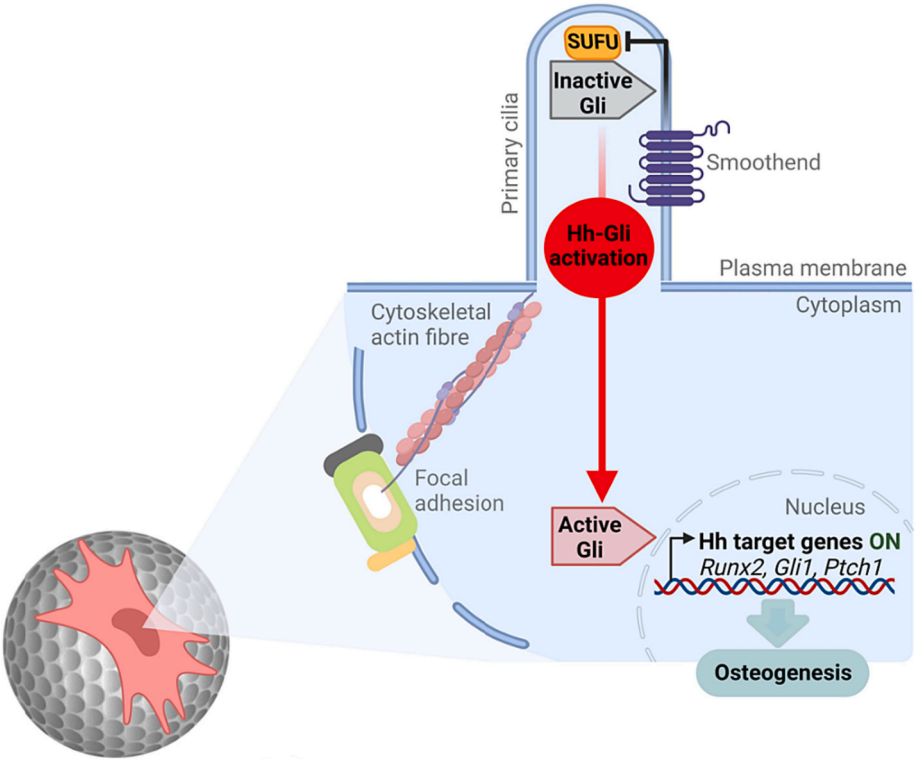

Fig. 8. Schematic depicting the proposed mechanism underpinning the osteoinductive influence of 3D dimpled surface topographical features of PLA microparticles on C3H10T1/2 cells. Dimpled topographies are sensed by C3H10T1/2 cells, which leads to changes in cytoskeleton organisation and the formation of primary cilia. This facilitates the activation of the Hedgehog signalling pathway and translocation of active Gli1 into the nucleus, where it upregulates the expression of Hh-and osteogenic-related genes, leading to the expression of early and late markers of osteogenesis. Image was created using Biorender.com.
Abbreviations: Hh, Hedgehog signalling pathway; Gli1, glioma associated oncogene homolog 1; Runx2, Runt-related transcription factor2; Ptch1, Patched 1.

observed with synovial mesenchymal stem cells reported in a recent study, which were suggested to have roles in mechanosensing and cell-matrix interactions [56].

Changes in topography are known to induce actin cytoskeletal changes [57]. Vinculin is a ubiquitously expressed mechanosensitive protein that interacts with F-actin during the recruitment of actin filaments to the growing focal adhesions, along with being involved in capping of actin filaments to control actin dynamics [58]. We demonstrated that C3H10T1/2 cells cultured on smooth surfaces showed diffuse perinuclear vinculin staining (Fig. 3), in agreement with previous studies on C3H10T1/2 and human fibroblasts h-TERT immortalised BJ1 cells [59,60]. Zhoa *et al.* reported that C3H10T1/2 cells displayed reduced levels of vinculin staining on hydroxyapatite-based multilayers, resulting in enhanced osteogenic differentiation [59]. The disorganised focal adhesion staining observed in C3H10T1/2 cells cultured on dimpled topographies is visibly similar to the disruption of focal adhesion assembly observed with oestrogen withdrawal in murine osteocyte-like cells, which resulted in primary cilia formation [54]. Micro-scale topographical features can block cell spreading by directly interfering with the establishment and maturation of focal adhesions [61]. Disrupted focal adhesions leads to actin depolymerisation and inhibit actin contractility [54,62], which was found to promote ciliogenesis [63]. Furthermore, Zhang *et al.* reported that introducing microscale topographies to 2D discs induced osteogenesis of hMSCs and caused changes in actin organisation coupled with ciliogenesis [38]. Therefore, the 3D dimpled topographies may cause differential assembly of focal adhesions in smooth versus dimpled microparticles, leading to cytoskeletal remodelling and ciliogenesis. This aligns with previous research reporting that actin cytoskeleton organisation can be modulated by designing specific surface topographical features that mimic ECM properties [57,64].

The formation of primary cilia exclusively in C3H10T1/2 cells cultured on dimpled microparticles was confirmed by immunostaining for ARL13B, a ciliary membrane marker (Fig. 4). Ciliogenesis can be promoted via changes in the expression of actin regulatory factors essential for branched actin network formation [65]. Changes in cell morphology can also have a strong influence on the formation of cilia [66,67]. It has been reported that cilia formation and length can be affected by sub-micron topographies (i.e. <10 μm) in MSCs [38]. The primary cilium is known to be essential for the transduction of the Hh signalling pathway in vertebrates [46,68], with important roles in mesenchymal cell mechanobiology and mechanotransduction [35,69,70]. Alterations in primary cilia structure or function directly influences osteogenesis via the modulation of Hh signalling pathway [54], which is indispensable in the early stages of osteogenesis and subsequent osteoblast maturation [12,71].

Our data demonstrated that C3H10T1/2 mesenchymal progenitor cells cultured on dimpled microparticles underwent osteogenesis in the absence of exogenous supplements, which was confirmed by the increase in the expression levels of osteogenesis-related genes representing early and late markers of osteogenesis, including *Runx2* and OCN (encoded by *Bglap2*), compared to cells cultured on smooth microparticles and 2D controls (Fig. 5). Runx2 is an important marker of early osteogenic differentiation [19,72]. Activation of Hh signalling pathway leads to direct induction of *Runx2* transcription [73], which further activates the Hh pathway through the induction of *Gli1* and *Ptch1* [74]. Expression of *Bglap2*, which serves as a late marker of osteogenic differentiation [75], was also upregulated. Culture of C3H10T1/2 cells on dimpled microparticles displayed a significant increase in *Bglap2* expression at day 3 post-seeding, which persisted to day 7. This aligns with our previous study using human MSCs, where we demonstrated that topographically-textured 3D microparticles can induce osteogenic differentiation of human MSCs *in vitro* [2]. Though PLA lacks intrinsic osteo-inductivity [76,77], previous studies have reported that stiffness can stimulate osteogenic differentiation to some degree [2,78]. This can explain the increase in expression levels of *Bglap2* also observed on smooth microparticles at day 7 post-seeding (Fig. 5). However, this was still significantly lower than expression levels of these markers by the cells cultured on dimpled microparticles.

Increasing evidence has demonstrated the crucial roles of Hh signalling in various bone development processes [79–81]. It is well-known that Hh signalling is mechano-responsive and required for loading-induced osteogenesis in MSCs [12]. Recent studies have increasingly focused on the potential role of the Hh pathway in response to mechanical cues [12,82–86]. The influence of different mechanical cues on Hh signalling pathway has also been reported, such as cyclic tensile strain [82–84], hydrostatic loading [85,86], oscillatory fluid flow [12] and matrix stiffness [87]. Previous studies that have reported the influence of topographical features on Hh signalling activation were mostly conducted using planar titanium surfaces [19,88]. Recent studies have shown that introducing planar topographies on titanium surfaces increased the expression of Hh-related genes [19,88,89]. Our data showed that dimpled microparticles significantly upregulated the activity of the canonical Hh pathway, demonstrated by the increase in expression levels of *Gli1* and *Ptch1*, and supported by the upregulation of *Smo* levels compared to smooth microparticles and 2D cultures (Fig. 6). This causal relationship between Hh pathway activation and osteogenic gene expression demonstrated here is consistent with previous findings, which showed increased expression of *Runx2* and *Bglap2* when the Hh pathway was chemically activated in MSC by purmorphamine treatment [40,90] and by using a recombinant N-SHH, which increased ALP activity [91]. Remarkably, dimpled microparticles enhanced Hh signalling at day 3 after seeding to a level similar to that observed for 2D cultures treated with 2 μM purmorphamine (Fig. 6). This highlights the potential of employing dimpled microparticles as a physical alternative to biochemical Hh agonists in research. The increased expression of Smo observed in dimpled microparticles agrees with a previous study that utilised rough titanium surfaces to culture osteoblast-like MG63 cells [19], reporting that surface topographies enhanced the expression levels of Hh-related genes including *Smo*. This represents an exciting avenue for future research to shed further light on the mechanism by which topography enhances Smo expression. It is well-established that Smo in the presence of primary cilia can drive activation of Hh signalling [47]. Smo translocates to the primary cilia in response to Hh ligands, with its activation promoting the release of Gli proteins from their carrier protein, Suppressor of Fused (Sufu). Direct transcriptional targets of Hh signalling include Gli1 and Ptch1 [53,92] (Fig. 8).

To demonstrate the role of Hh signalling in the osteo-inductive capabilities of 3D dimpled topographies investigated herein, we suppressed canonical Hh signalling using the Smo inhibitor KAAD-cyclopamine, subsequently quantifying osteogenesis-related gene expression. Our results demonstrated that KAAD-cyclopamine suppressed Hh activity and prevented the expression of the osteogenesis-related genes (*Runx2* and *Bglap2*) in C3H10T1/2 cells cultured on dimpled microparticles (Fig. 7). In contrast to previous studies that reported potential interactions between KAAD-cyclopamine and the utilised nanotopography-presenting titanium surfaces [93], our findings showed that KAAD-cyclopamine does not influence the cells cultured on the smooth microparticles. This data confirmed our hypothesis that Hedgehog–Gli signalling mediates the osteo-inductive impact of dimpled microparticles on C3H10T1/2 cells without the titanium-related constraints which may have impacted previous studies [19,93].

Unlike dimpled microparticles-based cultures, the expression levels of *Bglap2* observed at day 7 with smooth microparticle cultures is independent of Smo. This suggests the involvement of different osteogenesis-related signalling pathways in the promotion of osteogenesis, such as Wnt, TGFβ, bone morphogenic protein (BMP) or Notch signalling pathways, potentially mediated by PLA surface stiffness [94–96].

In summary, we provide novel mechanistic insights into the osteo-inductive influence of dimpled topographical design of PLA microparticles, demonstrating that the osteoinductive effect of these dimpled

microparticles is mediated by Hedgehog signalling, and that the route of activation of the Hh-Gli1 pathway is Smo-dependent (Fig. 7). The incorporation of tailored micro-materials in developmental bioengineering applications provides new opportunities to manipulate self-organisation from within a developing construct with high reproducibility and reliability, for example within organoids and tissue-engineered 3D constructs. These micron-sized, readily injectable surface-engineered microparticles offer significant potential in bone regenerative applications and can be used in modelling diseases for which Hh signalling dysfunction is implicated without the need for adding exogenous agonists.

5. Conclusion

This study uncovers novel mechanistic insights into the osteoinductive impact of 3D topographical patterning of microparticles on the modulation of Hh signalling – a key pathway in cellular differentiation. Our findings will provide key guiding parameters for designing microparticle-based models that mimic key cellular and molecular regulation of Hh signalling in bone development and regeneration.

There is growing interest in the development of advanced culture substrates that can direct endogenous signalling pathways. Currently, researchers need to compromise between complexity and control in *in vitro* stem cell differentiation. When control over differentiation is needed, only limited complexity in cellular composition and culture media supplementation is possible. Alternatively, a high degree of complexity in cellular composition limits the ability to control individual cell fates, typically due to the need for utilisation of a common culture media. Tailoring the architectural features of microparticles as modular culture substrates will allow the assembly of cell-microparticle aggregates as modular building blocks. Modular scaffolds can be prepared by assembling varying topographical designs of polylactic acid-based microparticles as building blocks to create novel Hh-related disease model systems free from confounding biochemical factors that are typically added to induce differentiation *in vitro*. This will open avenues for engineering spatially controlled, heterogeneous tissue constructs as advanced *in vitro* experimental systems suitable for *in vitro* discovery research and high-throughput screening of novel drug candidates for treating diseases for which Hh signalling dysfunction is associated.

CRediT authorship contribution statement

FG: Methodology, Data curation, Investigation, Formal analysis, Writing-original draft, Writing-review & editing, Funding acquisition; **LS:** Methodology, Data curation of BET surface area measurements, Investigation, Writing-review & editing, **CJ:** Supervision, Resources, Writing-review & editing; **NDG:** Supervision, Resources, Writing-review & editing; **MA:** Conceptualization, Supervision, Project administration, Funding acquisition, Writing-original draft, Writing-review & editing.

All authors have given approval to the final version of the manuscript.

Declaration of competing interest

The authors declare that they have no known competing financial interests or personal relationships that could have appeared to influence the work reported in this paper.

Data availability

Data will be made available on request.

Acknowledgements

MA acknowledges funding by a University Academic Fellowship (University of Leeds, UK). FG is supported by a scholarship from Kuwait University, Kuwait. We thank Dr. Ruth Hughes from the Faculty of Biological Sciences Bioimaging facility for support with the Zeiss LSM880 Airyscan confocal microscope, funded by a Wellcome Trust (WT104918MA). We thank John Harrington and Stuart Micklethwaite from Leeds Electron Microscopy and Spectroscopy Centre (LEMAS) for their support. Finally, we acknowledge Tayah Hopes for her invaluable support with RT-qPCR, Dr. Iain Manfield (Wellcome Trust-funded Biomolecular Interactions Facility, Astbury Centre; 062164/Z/00/Z), and Helena Brown (Sorby Environmental Fluid Dynamics Laboratory). For the purpose of open access, the authors have applied a creative commons attribution (CC BY) public copyright licence to any Author Accepted Manuscript version arising from this submission.

Appendix A. Supplementary data

Supplementary data to this article can be found online at https://doi.org/10.1016/j.bioadv.2023.213652.

References

[1] S.-Y. Lee, I.-S. Koo, H.J. Hwang, D.W. Lee, *In vitro* three-dimensional (3D) cell culture tools for spheroid and organoid models, SLAS Discov. 28 (2023) 119–137, https://doi.org/10.1016/j.slasd.2023.03.006.

[2] M.H. Amer, M. Alvarez-Paino, J. McLaren, F. Pappalardo, S. Trujillo, J.Q. Wong, S. Shrestha, S. Abdelrazig, L.A. Stevens, J.B. Lee, et al., Designing topographically textured microparticles for induction and modulation of osteogenesis in mesenchymal stem cell engineering, Biomaterials 266 (2021) 120450.

[3] A.-N. Cho, Y. Jin, Y. An, J. Kim, Y.S. Choi, J.S. Lee, J. Kim, W.-Y. Choi, D.-J. Koo, W. Yu, et al., Microfluidic device with brain extracellular matrix promotes structural and functional maturation of human brain organoids, Nat. Commun. 12 (2021) 4730.

[4] F. Puza, S. Rostami, B. Özçolak-Aslan, S. Odabaş, K.D. Jandt, B. Garipcan, Anisotropic bone surface topography mimicked chitosan/graphene oxide membranes, Adv. Eng. Mater. 25 (2023) 2200777, https://doi.org/10.1002/adem.202200777.

[5] F. Guilak, D.M. Cohen, B.T. Estes, J.M. Gimble, W. Liedtke, C.S. Chen, Control of stem cell fate by physical interactions with the extracellular matrix, Cell Stem Cell 5 (2009) 17–26.

[6] X. Liu, Z. Ren, X. Meng, Y. Xu, Substrate topography regulates extracellular matrix component secretion by bone marrow-derived mesenchymal stem cells, J. Sci. Adv. Mater. Devices 7 (2022) 100437, https://doi.org/10.1016/j.jsamd.2022.100437.

[7] C.C. DuFort, M.J. Paszek, V.M. Weaver, Balancing forces: architectural control of mechanotransduction, Nat. Rev. Mol. Cell Biol. 12 (2011) 308–319.

[8] G. Abagnale, M. Steger, V.H. Nguyen, N. Hersch, A. Sechi, S. Joussen, B. Denecke, R. Merkel, B. Hoffmann, A. Dreser, et al., Surface topography enhances differentiation of mesenchymal stem cells towards osteogenic and adipogenic lineages, Biomaterials 61 (2015) 316–326, https://doi.org/10.1016/j.biomaterials.2015.05.030.

[9] J.K. Chaudhary, P.C. Rath, Microgrooved-surface topography enhances cellular division and proliferation of mouse bone marrow-derived mesenchymal stem cells, PloS One 12 (2017), e0182128.

[10] M.P. Bernardo, B.C.R. da Silva, A.E.I. Hamouda, M.A.S. de Toledo, C. Schalla, S. Rütten, R. Goetzke, L.H.C. Mattoso, M. Zenke, A. Sechi, PLA/hydroxyapatite scaffolds exhibit *in vitro* immunological inertness and promote robust osteogenic differentiation of human mesenchymal stem cells without osteogenic stimuli, Sci. Rep. 12 (2022) 2333.

[11] B. Koh, N. Sulaiman, M.B. Fauzi, J.X. Law, M.H. Ng, R.B.H. Idrus, M.D. Yazid, Three dimensional microcarrier system in mesenchymal stem cell culture: a systematic review, Cell Biosci. 10 (2020) 75.

[12] G.P. Johnson, S. Fair, D.A. Hoey, Primary cilium-mediated MSC mechanotransduction is dependent on Gpr161 regulation of hedgehog signalling, Bone 145 (2021) 115846, https://doi.org/10.1016/j.bone.2021.115846.

[13] Y. Shi, J. Chen, C.M. Karner, F. Long, Hedgehog signaling activates a positive feedback mechanism involving insulin-like growth factors to induce osteoblast differentiation, Proc. Natl. Acad. Sci. 112 (2015) 4678–4683.

[14] R. Teperino, F. Aberger, H. Esterbauer, N. Riobo, J.A. Pospisilik, Canonical and non-canonical hedgehog signalling and the control of metabolism, Semin. Cell Dev. Biol. 33 (2014) 81–92.

[15] H. Zhou, L. Zhang, Y. Chen, C.-H. Zhu, F.-M. Chen, A. Li, Research progress on the hedgehog signalling pathway in regulating bone formation and homeostasis, Cell Prolif. 55 (2022), e13162, https://doi.org/10.1111/cpr.13162.

[16] R. Tevlin, E.Y. Seo, O. Marecic, A. McArdle, X. Tong, B. Zimdahl, A. Malkovskiy, R. Sinha, G. Gulati, X. Li, et al., Pharmacological rescue of diabetic skeletal stem cell niches, Sci. Transl. Med. 9 (2017).

[17] H. Takebe, N. Shalehin, A. Hosoya, T. Shimo, K. Irie, Sonic hedgehog regulates bone fracture healing, Int. J. Mol. Sci. 21 (2020) 677.

[18] Y. Kitaura, H. Hojo, Y. Komiyama, T. Takato, U.I. Chung, S. Ohba, Gli1 haploinsufficiency leads to decreased bone mass with an uncoupling of bone metabolism in adult mice, PloS One 9 (2014), e109597.

[19] Y. Lin, Y. Huang, J. He, F. Chen, Y. He, W. Zhang, Role of Hedgehog-Gli1 signaling in the enhanced proliferation and differentiation of MG63 cells enabled by hierarchical micro-/nanotextured topography, Int. J. Nanomedicine 12 (2017) 3267–3280.

[20] Y. Lin, Y. Shao, J. Li, W. Zhang, K. Zheng, X. Zheng, X. Huang, Z. Liao, Y. Xie, J. He, The hierarchical micro-/nanotextured topographies promote the proliferation and angiogenesis-related genes expression in human umbilical vein endothelial cells by initiation of Hedgehog-Gli1 signaling, Artif. Cells Nanomed. Biotechnol. 46 (2018) S1141–S1151.

[21] Y. Xie, X. Chen, X. Zheng, L. Li, J. Li, Y. Xu, J. He, Y. Lin, Beta1-integrin/Hedgehog-Gli1 signaling pathway fuels the diameter-dependent osteoblast differentiation on different TiO(2) nanotubes: the optimal-diameter nanotubes for osteoblast differentiation, Int. J. Biochem. Cell Biol. 137 (2021) 106026.

[22] R.J. Miron, Y. Shuang, D.D. Bosshardt, J. Caballé-Serrano, F. Chandad, Y. Zhang, Osteogenic gene array of osteoblasts cultured on a novel osteoinductive biphasic calcium phosphate bone grafting material, Clin. Oral Investig. 21 (2017) 801–808.

[23] L. Ru, B. Pan, J. Zheng, Signalling pathways in the osteogenic differentiation of periodontal ligament stem cells, Open Life Sci. 18 (1) (2023), 20220706, https://doi.org/10.1515/biol-2022-0706.

[24] K.-J. Chao, P.-H. Liu, K.-Y. Huang, Thin films of mesoporous silica: characterization and applications, C. R. Chim. 8 (2005) 727–739, https://doi.org/10.1016/j.crci.2005.01.004.

[25] C.-Y. Chiu, A.S.T. Chiang, K.-J. Chao, Mesoporous silica powders and films—pore size characterization by krypton adsorption, Microporous Mesoporous Mater. 91 (2006) 244–253, https://doi.org/10.1016/j.micromeso.2005.12.003.

[26] K.J. Livak, T.D. Schmittgen, Analysis of relative gene expression data using real-time quantitative PCR and the 2(−Delta Delta C(T)) method, Methods 25 (2001) 402–408.

[27] L. Zhao, G. Li, K.M. Chan, Y. Wang, P.F. Tang, Comparison of multipotent differentiation potentials of murine primary bone marrow stromal cells and mesenchymal stem cell line C3H10T1/2, Calcif. Tissue Int. 84 (2009) 56–64.

[28] E. Stavenschi, M.N. Labour, D.A. Hoey, Oscillatory fluid flow induces the osteogenic lineage commitment of mesenchymal stem cells: the effect of shear stress magnitude, frequency, and duration, J. Biomech. 55 (2017) 99–106.

[29] S. Pirkmajer, A.V. Chibalin, Serum starvation: caveat emptor, Am. J. Physiol. Cell Physiol. 301 (2011) C272–C279, https://doi.org/10.1152/ajpcell.00091.2011.

[30] J.K. Ching, P. Rajguru, N. Marupudi, S. Banerjee, J.S. Fisher, A role for AMPK in increased insulin action after serum starvation, Am. J. Physiol. Cell Physiol. 299 (2010) C1171–C1179.

[31] A. Klip, G. Li, W.J. Logan, Induction of sugar uptake response to insulin by serum depletion in fusing L6 myoblasts, Am. J. Physiol. Endocrinol. Metab. 247 (1984) E291–E296.

[32] E.H. Lin, Y.R. Kao, C.A. Lin, T.Y. Kuo, S.P. Yang, C.F. Hsu, T.Y. Chou, C.C. Ho, C. W. Wu, Hedgehog pathway maintains cell survival under stress conditions, and drives drug resistance in lung adenocarcinoma, Oncotarget 7 (2016) 24179–24193.

[33] M.A. Schwartz, Integrins and extracellular matrix in mechanotransduction, Cold Spring Harb. Perspect. Biol. 2 (2010) a005066.

[34] M.D. Welch, R.D. Mullins, Cellular control of actin nucleation, Annu. Rev. Cell Dev. Biol. 18 (2002) 247–288.

[35] D.A. Hoey, S. Tormey, S. Ramcharan, F.J. O'Brien, C.R. Jacobs, Primary cilia-mediated mechanotransduction in human mesenchymal stem cells, Stem Cells 30 (2012) 2561–2570.

[36] L. McNamara, Bone as a material, in: P. Ducheyne (Ed.), Comprehensive Biomaterials, Elsevier, 2011, pp. 169–186, https://doi.org/10.1016/B978-0-08-055294-1.00068-4.

[37] V. Cantagrel, J.L. Silhavy, S.L. Bielas, D. Swistun, S.E. Marsh, J.Y. Bertrand, S. Audollent, T. Attié-Bitach, K.R. Holden, W.B. Dobyns, et al., Mutations in the cilia gene ARL13B lead to the classical form of Joubert syndrome, Am. J. Hum. Genet. 83 (2008) 170–179.

[38] J. Zhang, M.T. Dalbay, X. Luo, E. Vrij, D. Barbieri, L. Moroni, J.D. de Bruijn, C. A. van Blitterswijk, J.P. Chapple, M.M. Knight, H. Yuan, Topography of calcium phosphate ceramics regulates primary cilia length and TGF receptor recruitment associated with osteogenesis, Acta Biomater. 57 (2017) 487–497, https://doi.org/10.1016/j.actbio.2017.04.004.

[39] T.M. Liu, E.H. Lee, Transcriptional regulatory cascades in Runx2-dependent bone development, Tissue Eng. Part B Rev. 19 (2013) 254–263.

[40] X. Wu, J. Walker, J. Zhang, S. Ding, P.G. Schultz, Purmorphamine induces osteogenesis by activation of the hedgehog signaling pathway, Chem. Biol. 11 (2004) 1229–1238.

[41] Y.T. Tsao, Y.J. Huang, H.H. Wu, Y.A. Liu, Y.S. Liu, O.K. Lee, Osteocalcin mediates biomineralization during osteogenic maturation in human mesenchymal stromal cells, Int. J. Mol. Sci. 18 (2017).

[42] R. Petrova, A.L. Joyner, Roles for Hedgehog signaling in adult organ homeostasis and repair, Development 141 (2014) 3445–3457.

[43] A. Shimoyama, M. Wada, F. Ikeda, K. Hata, T. Matsubara, A. Nifuji, M. Noda, K. Amano, A. Yamaguchi, R. Nishimura, T. Yoneda, Ihh/Gli2 signaling promotes osteoblast differentiation by regulating Runx2 expression and function, Mol. Biol. Cell 18 (2007) 2411–2418, https://doi.org/10.1091/mbc.e06-08-0743.

[44] S.R. Montgomery, T. Nargizyan, V. Meliton, S. Nachtergaele, R. Rohatgi, F. Stappenbeck, M.E. Jung, J.S. Johnson, B. Aghdasi, H. Tian, et al., A novel osteogenic oxysterol compound for therapeutic development to promote bone growth: activation of hedgehog signaling and osteogenesis through smoothened binding, J. Bone Miner. Res. 29 (2014) 1872–1885, https://doi.org/10.1002/jbmr.2213.

[45] J.K. Chen, J. Taipale, M.K. Cooper, P.A. Beachy, Inhibition of hedgehog signaling by direct binding of cyclopamine to smoothened, Genes Dev. 16 (2002) 2743–2748.

[46] G. Wheway, L. Nazlamova, J.T. Hancock, Signaling through the primary cilium, Front. Cell Develop. Biol. 6 (2018).

[47] R. Rohatgi, L. Milenkovic, R.B. Corcoran, M.P. Scott, Hedgehog signal transduction by smoothened: pharmacologic evidence for a 2-step activation process, Proc. Natl. Acad. Sci. 106 (2009) 3196–3201, https://doi.org/10.1073/pnas.0813373106.

[48] M. Alvarez-Paino, M.H. Amer, A. Nasir, V. Cuzzucoli Crucitti, J. Thorpe, L. Burroughs, D. Needham, C. Denning, M.R. Alexander, C. Alexander, F.R.A. J. Rose, Polymer microparticles with defined surface chemistry and topography mediate the formation of stem cell aggregates and cardiomyocyte function, ACS Appl. Mater. Interfaces 11 (2019) 34560–34574.

[49] L.A. Gurski, N.J. Petrelli, X. Jia, M.C. Farach-Carson, 3D matrices for anti-cancer drug testing and development, Oncol. Issues 25 (2010) 20–25.

[50] B. Fallica, J.S. Maffei, S. Villa, G. Makin, M. Zaman, Alteration of cellular behavior and response to PI3K pathway inhibition by culture in 3D collagen gels, PloS One 7 (2012), e48024.

[51] A.G. Souza, I.B.B. Silva, E. Campos-Fernandez, L.S. Barcelos, J.B. Souza, K. Marangoni, L.R. Goulart, V. Alonso-Goulart, Comparative assay of 2D and 3D cell culture models: proliferation, gene expression and anticancer drug response, Curr. Pharm. Des. 24 (2018) 1689–1694.

[52] R. Chignola, A. Schenetti, G. Andrighetto, E. Chiesa, R. Foroni, S. Sartoris, G. Tridente, D. Liberati, Forecasting the growth of multicell tumour spheroids: implications for the dynamic growth of solid tumours, Cell Prolif. 33 (2000) 219–229.

[53] F.I. Ghuloum, C.A. Johnson, N.A. Riobo-Del Galdo, M.H. Amer, From mesenchymal niches to engineered *in vitro* model systems: exploring and exploiting biomechanical regulation of vertebrate hedgehog signalling, Mater. Today Bio 17 (2022) 100502.

[54] I.P. Geoghegan, L.M. McNamara, D.A. Hoey, Estrogen withdrawal alters cytoskeletal and primary ciliary dynamics resulting in increased Hedgehog and osteoclastogenic paracrine signalling in osteocytes, Sci. Rep. 11 (2021) 9272.

[55] A.B. Bernard, R.Z. Chapman, K.S. Anseth, Controlled local presentation of matrix proteins in microparticle-laden cell aggregates, Biotechnol. Bioeng. 111 (2014) (2014) 1028–1037.

[56] S. Suzuki, M. Mizuno, Y. Sakamaki, A. Mimata, K. Endo, Y. Kohno, N. Ozeki, K. Otabe, H. Katano, K. Tsuji, et al., Morphological changes in synovial mesenchymal stem cells during their adhesion to the meniscus, Lab. Invest. 100 (2020) 916–927.

[57] H. Miyoshi, T. Adachi, Topography design concept of a tissue engineering scaffold for controlling cell function and fate through actin cytoskeletal modulation, Tissue Eng. Part B Rev. 20 (2014) 609–627.

[58] C.E. Tolbert, K. Burridge, S.L. Campbell, Vinculin regulation of F-actin bundle formation: what does it mean for the cell? Cell Adh. Migr. 7 (2013) 219–225.

[59] M. Zhao, R. Anouz, T. Groth, Effect of microenvironment on adhesion and differentiation of murine C3H10T1/2 cells cultured on multilayers containing collagen I and glycosaminoglycans, J. Tissue Eng. 11 (2020) (2041731420940560).

[60] M.J. Dalby, S.J. Yarwood, Analysis of focal adhesions and cytoskeleton by custom microarray, Methods Mol. Biol. 370 (2007) 121–134.

[61] F. Robotti, S. Bottan, F. Fraschetti, A. Mallone, G. Pellegrini, N. Lindenblatt, C. Starck, V. Falk, D. Poulikakos, A. Ferrari, A micron-scale surface topography design reducing cell adhesion to implanted materials, Sci. Rep. 8 (2018) 10887.

[62] I.P. Geoghegan, D.A. Hoey, L.M. McNamara, Estrogen deficiency impairs integrin α(v)β(3)-mediated mechanosensation by osteocytes and alters osteoclastogenic paracrine signalling, Sci. Rep. 9 (2019) 4654.

[63] C.E.L. Smith, A.V.R. Lake, C.A. Johnson, Primary cilia, ciliogenesis and the actin cytoskeleton: a little less resorption, a little more actin please, Front. Cell Develop. Biol. 8 (2020), https://doi.org/10.3389/fcell.2020.622822.

[64] H.-Y. Lou, W. Zhao, X. Li, L. Duan, A. Powers, M. Akamatsu, F. Santoro, A. F. McGuire, Y. Cui, D.G. Drubin, B. Cui, Membrane curvature underlies actin reorganization in response to nanoscale surface topography, Proc. Natl. Acad. Sci. 116 (2019) 23143–23151, https://doi.org/10.1073/pnas.1910166116.

[65] J. Cao, Y. Shen, L. Zhu, Y. Xu, Y. Zhou, Z. Wu, Y. Li, X. Yan, X. Zhu, miR-129-3p controls cilia assembly by regulating CP110 and actin dynamics, Nat. Cell Biol. 14 (2012) 697–706.

[66] A. Pitaval, Q. Tseng, M. Bornens, M. Théry, Cell shape and contractility regulate ciliogenesis in cell cycle-arrested cells, J. Cell Biol. 191 (2010) 303–312.

[67] J.V. Shah, Cells in tight spaces: the role of cell shape in cell function, J. Cell Biol. 191 (2010) 233–236.

[68] F. Bangs, K.V. Anderson, Primary cilia and mammalian hedgehog signaling, Cold Spring Harb. Perspect. Biol. 9 (2017), https://doi.org/10.1101/cshperspect.a028175.

[69] J.C. Chen, D.A. Hoey, M. Chua, R. Bellon, C.R. Jacobs, Mechanical signals promote osteogenic fate through a primary cilia-mediated mechanism, FASEB J. 30 (2016) 1504–1511.

[70] G.P. Johnson, E. Stavenschi, K.F. Eichholz, M.A. Corrigan, S. Fair, D.A. Hoey, Mesenchymal stem cell mechanotransduction is cAMP dependent and regulated by adenylyl cyclase 6 and the primary cilium, J. Cell Sci. 131 (2018) jcs222737.

[71] S. Onodera, A. Saito, H. Hojo, T. Nakamura, D. Zujur, K. Watanabe, N. Morita, D. Hasegawa, H. Masaki, H. Nakauchi, et al., Hedgehog activation regulates human osteoblastogenesis, Stem Cell Rep. 15 (2020) 125–139, https://doi.org/10.1016/j.stemcr.2020.05.008.

[72] A. Al-Wahabi, T. Ser-Od, K. Inoue, K. Nakajima, K. Matsuzaka, T. Inoue, Topography enhances Runx2 expression in outgrowing cells from iPS cell-derived

embryoid bodies, J. Biomed. Mater. Res. B Appl. Biomater. 107 (2019) 2288–2296, https://doi.org/10.1002/jbm.b.34321.
[73] E.J. Kim, S.W. Cho, J.O. Shin, M.J. Lee, K.S. Kim, H.S. Jung, Ihh and Runx2/Runx3 signaling interact to coordinate early chondrogenesis: a mouse model, PloS One 8 (2013), e55296.
[74] T. Komori, Molecular mechanism of Runx2-dependent bone development, Mol. Cells 43 (2020) 168–175.
[75] M. Ikegame, S. Ejiri, H. Okamura, Expression of non-collagenous bone matrix proteins in osteoblasts stimulated by mechanical stretching in the cranial suture of neonatal mice, J. Histochem. Cytochem. 67 (2019) 107–116.
[76] B. Wildemann, F. Kandziora, G. Krummrey, N. Palasdies, N.P. Haas, M. Raschke, G. Schmidmaier, Local and controlled release of growth factors (combination of IGF-I and TGF-beta I, and BMP-2 alone) from a polylactide coating of titanium implants does not lead to ectopic bone formation in sheep muscle, J. Control. Release 95 (2004) 249–256, https://doi.org/10.1016/j.jconrel.2003.11.014.
[77] J. Wang, J. Guo, J. Liu, L. Wei, G. Wu, BMP-functionalised coatings to promote osteogenesis for orthopaedic implants, Int. J. Mol. Sci. 15 (2014) 10150–10168.
[78] Y. Deng, X. Liu, A. Xu, L. Wang, Z. Luo, Y. Zheng, F. Deng, J. Wei, Z. Tang, S. Wei, Effect of surface roughness on osteogenesis *in vitro* and osseointegration *in vivo* of carbon fiber-reinforced polyetheretherketone-nanohydroxyapatite composite, Int. J. Nanomedicine 10 (2015) 1425–1447.
[79] R. Jemtland, P. Divieti, K. Lee, G.V. Segre, Hedgehog promotes primary osteoblast differentiation and increases PTHrP mRNA expression and iPTHrP secretion, Bone 32 (2003) 611–620.
[80] C. Wicking, I. Smyth, A. Bale, The hedgehog signalling pathway in tumorigenesis and development, Oncogene 18 (1999) 7844–7851.
[81] H. Zhou, L. Zhang, Y. Chen, C.H. Zhu, F.M. Chen, A. Li, Research progress on the hedgehog signalling pathway in regulating bone formation and homeostasis, Cell Prolif. 55 (2022), e13162.
[82] R. Gao, C. Shi, C. Yang, Y. Zhao, X. Chen, X. Zhou, Cyclic stretch promotes the ossification of ligamentum flavum by modulating the Indian hedgehog signaling pathway, Mol. Med. Rep. 22 (2020) 1119–1128.
[83] C.L. Thompson, J.P. Chapple, M.M. Knight, Primary cilia disassembly down-regulates mechanosensitive hedgehog signalling: a feedback mechanism controlling ADAMTS-5 expression in chondrocytes, Osteoarthr. Cartil. 22 (2014) 490–498.
[84] D. Morrow, C. Sweeney, Y.A. Birney, S. Guha, N. Collins, P.M. Cummins, R. Murphy, D. Walls, E.M. Redmond, P.A. Cahill, Biomechanical regulation of hedgehog signaling in vascular smooth muscle cells *in vitro* and *in vivo*, Am. J. Phys. Cell Phys. 292 (2007) C488–C496, https://doi.org/10.1152/ajpcell.00337.2005.
[85] Y.Y. Shao, L. Wang, J.F. Welter, R.T. Ballock, Primary cilia modulate Ihh signal transduction in response to hydrostatic loading of growth plate chondrocytes, Bone 50 (2012) 79–84.
[86] L. Huang, X. Cai, H. Li, Q. Xie, M. Zhang, C. Yang, The effects of static pressure on chondrogenic and osteogenic differentiation in condylar chondrocytes from temporomandibular joint, Arch. Oral Biol. 60 (2015) 622–630, https://doi.org/10.1016/j.archoralbio.2015.01.003.
[87] T. Yu, K. Hu, Q. Xu, X. Xu, C. Du, Y. Zhao, S. Yan, W. Wang, S. Tang, S. Yue, et al., An easy-to-fabricate hydrogel platform with tunable stiffness and cell anchorage: validation of its feasibility in modulating sonic hedgehog signaling pathway physically, Macromol. Mater. Eng. 305 (2020) 1900759, https://doi.org/10.1002/mame.201900759.
[88] N. Donos, M. Retzepi, I. Wall, S. Hamlet, S. Ivanovski, *In vivo* gene expression profile of guided bone regeneration associated with a microrough titanium surface, Clin. Oral Implants Res. 22 (2011) 390–398.
[89] S.Y. Kim, J.Y. Yoo, J.Y. Ohe, J.W. Lee, J.H. Moon, Y.D. Kwon, J.S. Heo, Differential expression of osteo-modulatory molecules in periodontal ligament stem cells in response to modified titanium surfaces, Biomed. Res. Int. 2014 (2014) 452175.
[90] A. Shimoyama, M. Wada, F. Ikeda, K. Hata, T. Matsubara, A. Nifuji, M. Noda, K. Amano, A. Yamaguchi, R. Nishimura, T. Yoneda, Ihh/Gli2 signaling promotes osteoblast differentiation by regulating Runx2 expression and function, Mol. Biol. Cell 18 (2007) 2411–2418.
[91] J.Q. Cai, Y.Z. Huang, X.H. Chen, H.L. Xie, H.M. Zhu, L. Tang, Z.M. Yang, Y. C. Huang, L. Deng, Sonic hedgehog enhances the proliferation and osteogenic differentiation of bone marrow-derived mesenchymal stem cells, Cell Biol. Int. 36 (2012) 349–355.
[92] X. Guo, N.A. Riobo-Del Galdo, E.J. Kim, G.R. Grant, D.R. Manning, Overlap in signaling between smoothened and the α subunit of the heterotrimeric G protein G13, PloS One 13 (2018), e0197442.
[93] P.G. Souza, L.F. Adolpho, H.B. Lopes, D. Weffort, A.T.P. Souza, F.S. Oliveira, A. L. Rosa, M.M. Beloti, Effects of modulation of the hedgehog and notch signaling pathways on osteoblast differentiation induced by titanium with nanotopography, J. Funct. Biomater. 14 (2023) 79.
[94] J. Kopf, A. Petersen, G.N. Duda, P. Knaus, BMP2 and mechanical loading cooperatively regulate immediate early signalling events in the BMP pathway, BMC Biol. 10 (2012) 37.
[95] J. Cui, Y. Yang, P. Chen, R. Hang, Y. Xiao, X. Liu, L. Zhang, H. Sun, L. Bai, Differential nanoscale topography dedicates osteocyte-manipulated osteogenesis via regulation of the TGF-β signaling pathway, Int. J. Mol. Sci. 23 (2022) 4212.
[96] N. Chakravorty, S. Hamlet, A. Jaiprakash, R. Crawford, A. Oloyede, M. Alfarsi, Y. Xiao, S. Ivanovski, Pro-osteogenic topographical cues promote early activation of osteoprogenitor differentiation via enhanced TGFβ, Wnt, and Notch signaling, Clin. Oral Implants Res. 25 (2014) 475–486, https://doi.org/10.1111/clr.12178.